A vorticity streamfunction formulation for turbulent airfoil flows

Christensen, Henrik Frans

Publication date:
1993

Document Version
Publisher's PDF, also known as Version of record

RISØ

OBJECTIVE

The objective of Risø National Laboratory is to further technological development in three main areas: energy, environment and materials.

USERS

Risø's scientific results are widely applied in industry, agriculture and public services. Risø contributes its share of new knowledge to the global research community.

RESEARCH PROFILE

Risø emphasises long-term and strategic research providing a solid scientific foundation for the technological development of society.

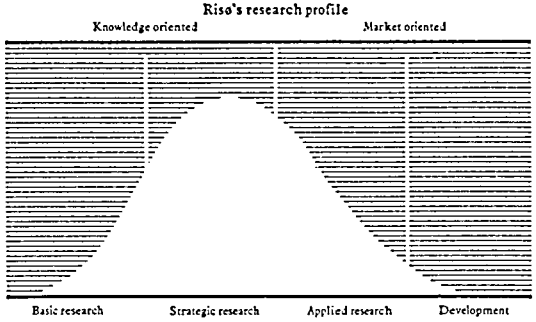

PRIORITY AREAS

* Combustion and gasification
* Wind energy
* Energy materials
* Energy and environmental planning
* Assessment of environmental loads
* Reduction of environmental loads
* Safety and reliability of technical systems
* Nuclear safety
* Atomic structure and properties of materials
* Advanced materials and materials technologies
* Optics and fluid dynamics

Risø-R-740(EN)
ISBN 87-550-1966-8
ISSN 0106-2840

Available on request from:
Risø Library
Risø National Laboratory
P.O. Box 49, DK-4000 Roskilde, Denmark
Phone +45 46 77 46 77, ext. 4004/4005
Telex 43116, Telefax 46 75 56 27

FHR.

RISØ

Risø-R-740(EN)

A vorticity - streamfunction formulation for turbulent airfoil flows

Henrik Frans Christensen

Risø National Laboratory, Roskilde, Denmark
December 1993

Risø–R–740(EN)

A vorticity - streamfunction formulation for turbulent airfoil flows

Henrik Frans Christensen

Risø National Laboratory, Roskilde, Denmark
December 1993

Abstract This Ph.D. thesis presents a vorticity - streamfunction formulation for turbulent airfoil flows. From the time averaged Navier -Stokes equation on a cartesian pressure - velocity form a vorticity - streamfunction formulation is derived in general curvelinear coordinates. A zero equation model, the Baldwin-Lomax model, is implemented to compute the turbulent viscosity. A second order implicit boundary condition has been applied for the vorticity at the wall. At a subsequent step the pressure field is computed by solving a transport equation for the stagnation pressure rather than solving a "traditional" Poisson equation. For low Reynolds numbers (laminar flow) the developed code has been evaluated on flows around cylinders and a NACA0012 airfoil and good agreement with literature is found. For high Reynolds numbers (attached turbulent flow) the code has been tested on a NACA0012 and shows good agreement with literature. Taking into account that the present formulation do not model transition , the code predicts well compared to other uncommercial and commercial Navier-Stokes codes.

Ph.D. thesis, jointly founded by Risø National Laboratory and The Danish Research Academy.

ISBN 87–550–1966-8
ISSN 0106–2840

Grafisk Service, Risø, 1994

Preface

As part of the demands to obtain a Ph.D. Degree this thesis is presented. The Ph.D. study has partly taken place at :

The Test Station for Wind Turbines (TSWT) in The Department for Meteorology and Wind Energy at Risø National Laboratory.

The Department for Fluid Mechanics (DFM) at The Technical University of Denmark.

and in

The Laboratory for Thermal Turbo Machinery (LTT) in The Fluid Section in The Department of Mechanical Engineering at the National Technical University of Athens, Greece.

The study has been under supervision of :

Professor, Ph.D. ***Poul Scheel Larsen***, (DFM)

Assistant Professor, Ph.D. ***Jens Nørkær Sørensen***, (DFM)

and

Senior Research Scientist, Ph.D. ***Helge Aagaard Madsen***, (TSWT)

Where coefficients and parameters are not defined and symbols not explained, when occuring in a context of the thesis, they can be found in the **List of symbols**.

Acknowledgements

The Ph.D. study and the thesis presented here has been founded jointly by Risø National Laboratory and The Danish Research Academy. I would like to express my thanks for this support.

I would also like to thank my two supervisors ***Jens Nørkær Sørensen*** and ***Helge Aagaard Madsen*** for being a source of inspiration and advice and for there patience with my impatience.

A special thank is given to Professor ***K. D. Papailiou***, who accepted my stay at The Laboratory for Thermal Turbo Machinery, at The Technical University of Athens

and

Dr. ***P. Chaviaropoulous*** for giving me many indispensable advices in our cooperation at the laboratory, and for showing me the Greek hospitality in the hours we spend together in Athens.

Finally my thanks go to my mother, ***Inger Kjær***, to whom this work is dedicated.

Contents

List of Figures

LIST OF SYMBOLS

All units are SI-units

A^+	26	[-]
$\underline{A}$	Matrix A	
b	Vector b	
c	Chord	[m],[-]
C_{CP}	1.6	[-]
C_{WK}	0.25	[-]
C_F	Total friction coefficient	[-]
C_L	Lift coefficient , $\frac{2L}{\rho c V^2}$	[-]
C_{KLEB}	Klebanov coefficient , 0.3	[-]
C_{MUTM}	14	[-]
C_N	Normal coefficient	[-]
C_P	Pressure coefficient, $\frac{2(p_0-p)}{\rho V^2}$	[-]
F,f	Function	
F_{KLEB}	Klebanov intermittency factor	[-]
F_{WAKE}	Wake function	[-]
K	Clauser constant, 0.0168	[-]
l	Mixing length	[m],[-]
$\vec{n}$	Vector normal to the surface	
$\vec{s}$	Vector tangential to the surface	
p	Total pressure	[Pa]
p_0	Total pressure at farfield boundary = 0	[Pa]
R_k	Rate of convergence	
R^n	Recidual vector at time step n	
Re_L	Free stream Reynolds number	[-]
Re_T	Reynolds number equivalent to the reciprocal turbulent diffusivity coefficient ν_T	[-]
Δt	Discrete timestep	[-]
t	Time	[s],[-]
V	Cartesian velocity vector	

V	Length of cartesian velocity vector	
V_{DIF}	Difference between Max. and Min. velocity	
u	Velocity, cartesian x-component	[m/s],[-]
u_τ	friction velocity, $u_\tau = \sqrt{\frac{\tau_w}{\rho_w}}$	$[\frac{m^3}{s^2}]$
	total velocity in a fixed x-station	[m/s], [-]
v	Velocity, cartesian y-component	[m/s],[-]
v^1	Covariant velocity parallel to the first general coordinate -, ζ - direction	[m],[-]
v^2	Covariant velocity parallel to the second general coordinate -, η - direction	[m],[-]
x	Position along airfoil surface	[m],[-]
y	Normal distance to the airfoil surface	[m],[-]
y^+	$y^+ = \frac{\rho_w u_\tau y}{\mu_w}$	[-]
$y_{crossover}$	y value, normal to the airfoil surface, separating the inner and outer turbulence model	[m],[-]
P,p_t	Total pressure	[Pa],[-]

Greek

α	Relaxation parameter	[-]
δ_{ij}	Kronecker delta, $\delta = 1$ for i=j, $\delta = 0$ for i $\neq$ j	
τ	Shear stress	$[\frac{N}{m}]$
τ_w	Shear stress at the wall	$[\frac{N}{m}]$
κ	Von Karman constant, 0.4	[-]
μ	Dynamic viscosity	$[\frac{N-s}{m^2}]$
μ_T	Turbulent dynamic viscosity	$[\frac{N-s}{m^2}]$
ν	Kinematic viscosity	$[\frac{m^2}{s}]$
ν_T	Turbulent kinematic viscosity	$[\frac{m^2}{s}]$
ν_w	Kinematic viscocity at the wall	$[\frac{m^2}{s}]$
θ	Angle	[degree]
θ_s	Angle of separation	[degree]
ζ	1st general coordinate	[m],[-]
η	2nd general coordinate	[m],[-]
ψ	Streamfunction	[1/s],[-]
ω	Length of vorticity vector	[1/s]
ρ	Density	$[\frac{kg}{m^3}]$, [-]

Miscellaneous

$\wp$	Term containing 2nd order derivatives of ν_T

Subscripts

$-$	Matrix
i	Indicator of direction for 1st general coordinate
j	Indicator of direction for 2nd general coordinate
Max	Maximum value
Min	Minimum value
$wall$	Wall value
ζ	1st order derivative in ζ - direction
η	1st order derivative in η - direction

Superscripts

$'$	fluctuations
n	iteration step n
$n+1$	iteration step n + 1
$-$	time averaged value
i	Point i in ζ - direction
j	Point j in η - direction
$*$	Temporary value

Chapter 1

Introduction

In the recent years an increasing amount of work has been carried out in order to obtain knowledge of the behaviour of aerodynamics related to the Horisontal Axis Wind Turbines (HAWT's). To date knowledge has been gained from experimental setups of full scale wind turbines in natural conditions or test of wings/ wing sections in wind tunnels. This knowledge has been used to correct the empirical relations in the theoretical models. But basically the theoretical models has, so far, not gone through the same kind of rapid development, as the experiments on wind turbines has.

1.1 Theoretical models for HAWT's operating below stall.

The aerodynamic behaviour of wings and rotors plays an important role when designing/ optimizing wind turbines for e.g. power output, structural loads, life time etc.

When designing a rotor, analysis of performance is one of the first steps to take. The basic performance analysis focus on the aerodynamic behaviour of the steady or time averaged flow.

Today most researchers apply the blade element/ momentum (BEM) method for performance analysis. The BEM method has proven accurate for a wide variety of rotors and flow conditions [21]. The Blade Element/Momentum Method, which in detail is described in e.g. [15] or [18], consists in basic of the assumption that the rotor can be analyzed as a number of independent elements. The induced velocity at each element is found by performing a momentum balance for an annular control volume containing the blade element and the air bounded by the stream surface

extended upwind and downwind of the element. Using two-dimensional lift and drag coefficients[1] the aerodynamic forces on the element are calculated at the geometrical angle of attack of the blade element relative to the local flow velocity[2].

The basic BEM technique has a number of limitations which are normally encountered in wind turbine applications. Many of these limitations have been overcomed using empirical relations derived from helicopter, propeller and wind turbine experiences [21].

For example for high loading of the rotor the simple momentum balance is not valid and Glauerts empirical relation for induced velocities for high disk loading is included. Blade tip and hub losses are generally accounted for in BEM methods using the Prandtl relationship [18]. Effects of the rotor wake is modelled by some designers.

Models which account for the location of the rotor/ wind turbine in a natural environment is also applied. Effects of the natural environment is for example : Yaw errors caused by the changes in the direction of the wind. The boundary layer on the ground. The aerodynamic "shadow" of the tower of the wind turbine. Turbulence of the free wind.

In spite of the assumptions made in BEM theory, this method often predicts rotor performance with acceptable accuracy. In the cases examined by Van Grol [20] , the power and annual energy were predicted with an uncertainty of $\pm$ 8 percent. According to Butterfield [21] the greatest difficulty in obtaining accurate predictions *below stall* is determination of the appropriate airfoil section characteristics.

To remove restrictions with respect to the choice of airfoil sections[3], the designer of rotors need an accurate code to compute airfoil characteristics, for airfoils, where these are not given apriory.

Today a number of codes are available to predict the characteristic performance of airfoils. Among the most popular commercial codes is the "Eppler Code" by [16] and XFOIL by [14]. Both codes have facilities for *direct*[4] and *inverse*[5] computations.

The "Eppler Code" consists of a Panel[6] - and Boundary Layer Method, and XFOIL is a Panel and Integral Method. These methods are numerically cheap and predicts well for unseparated flows. For separated flows

[1]Two-dimensional lift and drag coefficients may be replaced by three-dimensional coefficients, when available.

[2]including induced velocity effects

[3]In the early days of rotor and wing design, the designer was some how restricted to apply airfoils where the characteristics were given by wind tunnel measurements

[4]From a specified geometry the airfoil behaviour is found.

[5]From a specified behaviour the optimum shape of an airfoil is found.

[6]See e.g. [11] for results obtained with a panel method.

predictions by XFOIL [29] shows good agreement with wind tunnel measurements on a designed wind turbine airfoil like the NTUA - airfoil(see e.g. fig. (6.15) and fig. (6.16)). For airfoils with leading edge separation the agreement with measurements is not so profound [4].

For turbulent airfoil flows with large regions of separation the parabolic Boundary Layer Methods do not model the highly elliptic separation zone appropriate. Because of the development of price and speed of todays computers[7] and the development of fast integration schemes, modelling of the flow around airfoils by applying Navier-Stokes equations is becoming an appropriate and more accurate alternative to the Boundary Layer Equations.

As part of a Ph.D. study this thesis presents a vorticity - streamfunction formulation of the Navier-Stokes equations to predict the flow field and airfoil section characteristics at high Reynolds numbers.

1.2 HAWT's operating in quasi-steady stall.

Above stall rotor performance codes applying 2 D airfoil characteristics predicts poor. For this quasi-steady stall situation these codes predicts power output considerably lower than measured values.

McCroskey and Yaggy [34] among others made investigations on the importance of delayed quasi-steady stall related to helicopters in forward flight. They predicted a spanwise flow generated by centrifugal pumping. This radial flow results in a Coriolis acceleration, which acts as a favorable pressure gradient in the chordwise direction ([21]).

Applying a 3 D boundary layer model with viscous - invicid interaction Sørensen [44] modelled a wing and predicted a 30 % increase in the maximum lift due to the radial flow and additional Coriolis pressure force.

These predictions initiated a serie of full scale experiments on HAWT wings in natural conditions.

Among those who have been carrying out full scale experiments on HAWT wings in natural conditions is e.g. Rasmussen et Al. [38], Butterfield [6] and Madsen et Al. [30].

By measuring power output and blade flap moment Rasmussen was able to reconstruct characteristics for the wing sections of the blade under test. The resulting characteristics for the wing sections were quite different from 2 D data (see fig. 1.1).

[7]There has been a development in application from Personal Computers to Work Stations (going from a speed of $\sim$ 0.5 to 15 MFLOPS in 4 years in the wind turbine R and D environment)

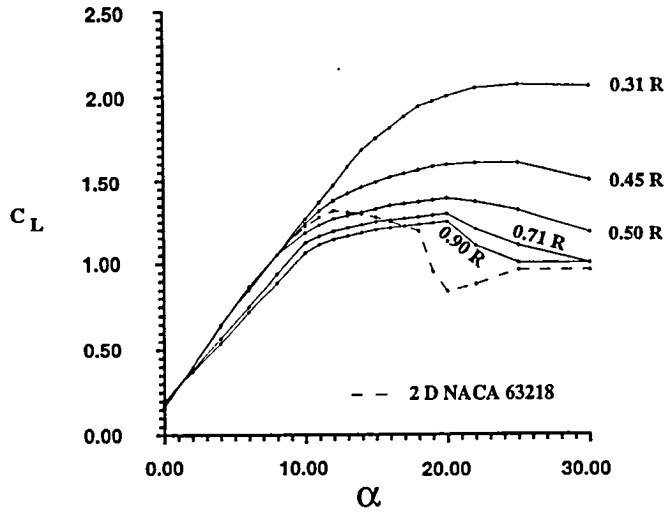

Figure 1.1: Predicted 3 D lift coefficient C_L versus α for 5 radial stations along a LM 10.5 m wing compared with 2 D wind tunnel data for a NACA 63218 airfoil.

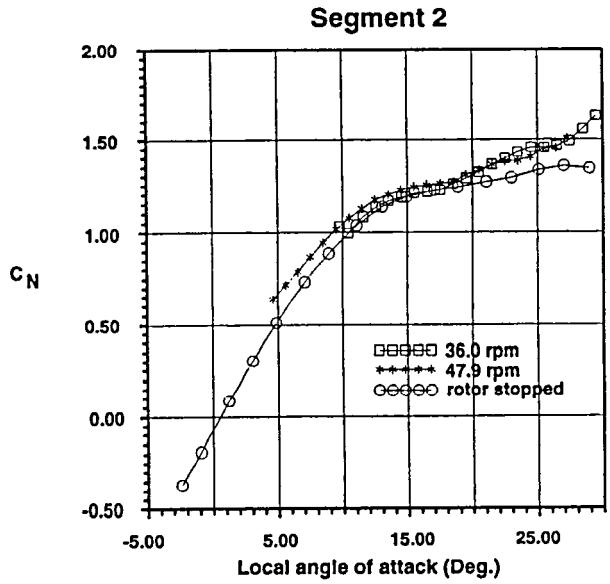

Figure 1.2: Normal force versus local angle of attack for the mid blade segment on a HAWT wing respectively rotating or stopped.

In order to get a more precise picture of the components of the quasi-steady stall phenomenon Butterfield [6] made a test setup measuring chord-wise surface pressure at different spanwise stations on a HAWT wing in natural condition.

A different experimental setup of a HAWT wing in natural conditions was done by Madsen et Al. [30] equiping 3 blade segments of a blade with force transducers. Madsen et Al. obtained measurements for the stationary and rotating wing operating in stall and out of stall separating the flow components in rotational -, 3 D - and unsteady effects (See fig. 1.2).

The results of Madsen et Al. confirmed the indication of significant differences in the characteristics for a rotating wings in stall and a 2 D airfoil.

One of the conclusions were, that if the mid section of the wing were respectively operating in stall with a rotating and a non rotating wing (fig.

1.2), the difference of the characteristics were neglectable, which lead to the conclusion that the differences between the characteristics of the mid section and 2 D airfoil , under these conditions seemed not to be caused by rotational effects but were related to the 3 D shape of the wing and the unsteady inflow. Recently this conclusion has been supported by wind tunnel measurements on a stationary wing, Madsen et Al. [33].

1.3 Unsteady aerodynamics for HAWT's.

A wind turbine in a natural environment will experience an unsteady aerodynamic flow field. When analysing blade loads on HAWT's unsteady effects are subdivided into dynamic stall and dynamic inflow. Dynamic stall considers unsteady aerodynamic effects in the immediate vicinity of the blade. Dynamic inflow refers to lagging in the response of the induced velocity field of a rotor following rapid changes in the rotor operating state. For example the mass of the air in the wake of the rotor makes it impossible for the wake to respond instantaneously to a change in rotor loading which can be observed after a change in blade pitch angle [21] .

Before 1988 unsteady aerodynamic effects were not included in load and performance analysis.

1.4 Dynamic stall

In 1988 the existence of dynamic stall and its effects on rotor loads were quantified by Butterfield [5] by meassuring pressure distribution on a 10 m HAWT. Dynamic stall was shown to occur under a variety of inflow conditions including turbulence, tower shadow and yawed flow.

Similar experiences were obtained by Madsen et Al. [32] on the test set up of blade segments on a HAWT wing previous mentioned. A typical hysteresis loop for a (C_L,α) - curve compared to a curve for quasi-stady stall can be seen in fig. (1.3).

Modelling of dynamic stall can be done by one of at least three models. The simplest and first proposed is the Gormont [19] model. From the angle of attack, the time rate change of the angle and 2 constants normally determined by experiments, the Gormont model determines an effective angle of attack which is responsable for the (C_L,α)- hysterese. The shape and the location of the hysterese relative to the quasi-steady stall curve is governed by the 2 constants. By determining the 2 constants Butterfield [21] found an adequate representation of the hysteresis observed at the outboard sections of the wing. For the mid section of the wing operating

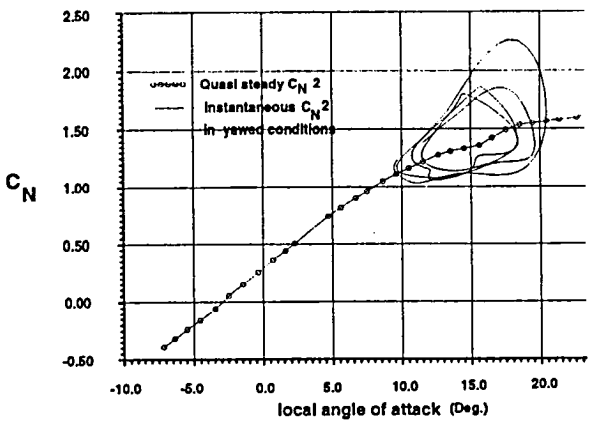

Figure 1.3: Quasi steady data for normal coefficient C_N versus local angle of attack for the mid blade segment 2 compared with instantaneous values measured with the rotor in yawed conditions.

in dynamic stall Madsen and Christensen [31] binned data for hysteresis at different mean angles of attack. The shapes of the hysteresis loops differs a lot at the different mean angle of attack. Predictions were made by the Gormont model, where the 2 model constants were adjusted to fit the measured hysterese shape at a mean angle of e.g. 17°. Applying the same constants, the Gormont model were used to predict the hysteresis at lower mean angles of attack. It was found that the model did not predict adequate hysterese shapes compared to the measurements.

1.5 Closure

As described in the previous sections a lot of interesting experimental and theoretical research has recently been done on airfoils, wings and rotors related to Horisontal Axis Wind Turbines.

The results from the experimental set up on wings has pointed the attention towards improvements of the theoretical modelling of 3 D - and rotational effects on a wing. But despite of the great interest for modelling the 3 D effects, there are still 2 D effects like the quasi-steady and dynamic stall, which are not fully understood and can't be modelled adequately today.

When it comes to modelling by Computational Fluid Dynamics (CFD) applying the Navier Stokes equations[8] obtaining a flow solution on a wing section (2 D) or a wing (3 D), there is a significant difference in the time a computer will apply in each case. Seen from a numerical point of view modelling in 2 D becomes very attractive.

As a consequence this Ph.D. study has been concentrated on the development of a two dimensional Navier-Stokes formulation to model the turbulent flow around airfoils designed for wind turbines.

[8] it can be argued that when it comes to modelling the strong separated spanwise flow on a rotationg wing at a Reynolds number of 2 - 3 mill. Viscous - Invicid interaction techniques, applying Boundary Layer Equations, are not succesfull as models, Cebeci [8]

Chapter 2

The system of governing flow equations for steady turbulent flows

The Navier-Stokes equations, which contains conservation of mass, momentum and energy, and can be found derived in e.g. [43] and [17] governs the motion of isotropic and Newtonian fluids[1] , to which group air belongs.

If the Navier Stokes equations, as they appear in [17], are solved to obtain a solution for e.g. a flow around an airfoil at a sufficient high Reynolds number, where turbulent motion occur, the result is termed a direct solution. Due to the limitations in todays computer memory and speed it is not possible to obtain direct solutions for flows at high Reynolds numbers.

On todays computers one can obtain a Direct Solution of the transition from laminar to turbulent flow on a flat plate at a Reynolds number of 5000 and in a 512^3 point cube ($\sim 1cm^3$) [35].

But the direct simulation as well as the Reynolds stress modelling[2] (second order models) of turbulence are despite of the fast development in computer power still not considered engineering turbulence models. For that reason they have not been considered in this work. This work just consider 1st order models.

[1] "A fluid is said to be *isotropic*, when the relation between the components of stress and those of the rate of strain is the same in all directions; it is said to be *Newtonian*, when this relation is linear", [43]

[2] Reynolds stress models model the Reynolds stresses without applying the Boussinesq assumption. In principle, it is possible to solve the time-dependent equations for the larger scales and to solve time averaged equations for the smaller scales with suitable modelling of the small scale structure.

2.1 The incompressible averaged Navier-Stokes equations on primitive form

In order to model turbulence with its stochastic nature one can apply a statistical approach, where the flow variables (u) is devided in a mean ($\overline{u}$) and a fluctuating component (u'). E.g. :

$$u = \overline{u} + u' \ , v = \overline{v} + v' \ , p = \overline{p} + p' \tag{2.1}$$

The time-averages are evaluated in a fixed point in space and e.g. given by :

$$\overline{u} = \frac{1}{t_1} \int_{t_0}^{t_0+t_1} \text{u dt} \tag{2.2}$$

The mean values are taken over a sufficiently long interval of time, t_1, to be completely independent of time, and the time-averaging of the fluctuations is zero by definition [43].

The time averaging of the Navier-Stokes equations gives, compared to the Navier-Stokes equation for laminar flows, raise to apparent or Reynolds stresses for the turbulent flow:

$$\tau_{ij} = -\rho \overline{u_i u_j} \tag{2.3}$$

As mensioned elsewhere, this work is concentrated on airflow in relation to wind turbines, and it is reasonable to assume incompressibility of this flow.

As a consequence the energy equation is eliminated in the governing flow equations.

The above mensioned circumstances lead to the following expression for the incompressible, averaged Navier-Stokes equations on the pressure - velocity (P-V) form (for simplicity, given here in cartesian coordinates, where the velocity components V_i for i = 1,2 correponds to the coordinate axis for the coordinates x_i. x_1 = x and x_2 = y) :

$$\frac{\partial V_i}{\partial x_i} = 0 \tag{2.4}$$

$$\frac{\partial V_j V_i}{\partial x_j} = -\frac{1}{\rho}\frac{\partial P}{\partial x_i} + \nu \nabla^2 V_i + \frac{1}{\rho}\frac{\partial \tau_{ij}}{\partial x_j} \tag{2.5}$$

ρ is the density of air, ν is the kinematic viscosity and τ_{ij} is the shear stress tensor.

In the last decades there has been a development of techniques for numerical integration of the turbulent incompressible Navier-Stokes equations. The most established, among them, are those formulations based on primitive variables like eq. (2.4) and eq. (2.5) and those using appropriate transformations, such as the vorticity- streamfunction one ($\omega - \psi$), which is by far the most used [37].

We will briefly discuss some of the advantages and disadvantages of these two types of formulations in the following section.

2.2 The incompressible averaged Navier-Stokes equations on the vorticity-streamfunction form

A method based on the solution of the primitive variables provide a better insight to the physical conservation laws and their boundary conditions. One of the great advantages is that two- and three-dimensional flows may be handled equally with similar algorithms. Turbulence models are straight forward to implement.

A primitive variable formulation for incompressible flows, however, suffer from the absence of a physically meaningful pressure equation. Often a Poisson type pressure equation (2.40) is used by applying the divergence operator on the momentum equation. Continuity is weakly satisfied,in this way, and inaccuracies may appear, especially when extra terms, like those of turbulence are present in the momentum equation.

A pressure correction technique can be applied [39] in order to assure a better fullfilment of the continuity equation.

Primitive variable formulations lead to velocity-pressure decoupling problems which appear when colocative discretization schemes are used. This odd-even decoupling [47] can be removed by staggering techniques, but the complexity of programming will be increased and the final solution will be affected in some extend.

The vorticity-streamfunction formulation is more suitable compared with primitive variables for representing the kinematic nature of the incompressible Navier-Stokes equations. The first advantage is related to the automatic satisfaction of the continuity due to the use of the streamfunction. The absence of the pressure gradient in the vorticity transport equation eliminates any problem related to odd- even decoupling and need for staggering.

Solving for flows including rotational effects (e.g. an ossilating airfoil) dosn't ask for additional terms for Coriolis - and Centrifugal forces in the

transport equation as a primitive formulation do. Rotational effects enter this solution through initial and boundary conditions [45].

Another advantages is that the closed form in which the equations appear in the $\psi - \omega$ formulation eq. (2.13) and eq. (2.14) , makes them suitable for applying fast numerical solvers as will be discussed in chapter 3.

These reasons make the $\psi - \omega$ formulation very attractive for accurate and fast solutions for high Reynolds, 2 D and/or axisymmetric Navier-Stokes equations.

Nevertheless a few drawbacks are still attributed to the $\psi - \omega$ formulations. The most important , among them, seems to be the difficulty in extending the method to 3 D. David et Al. [40] has tried to overcome these shortcomings and extended a $\psi - \omega$ method to 3 D. These attempts to make $\psi - \omega$ formulations competitive with primitive formulations in 3 D is to the authors knowledge still in its infancy. Because of this fact this analysis of high Reynolds flows related to wind turbines is limited to 2 D steady turbulent flows and unsteady laminar flows in this thesis.

An additional drawback is the necessity to use approximate and iterative vorticity boundary conditions along solid walls (see e.g. [46]).

2.3 Derivation of the equations in the vorticity-streamfunction formulation

In the following section we will derive the governing equations for incompressible Navier-Stokes flows on the vorticity - streamfunction formulation.

Obtaining the final equations in the $\psi - \omega$ formulation (eq. 2.13 and eq. 2.14) consists of the following steps :

- 1 *Definition of vorticity*
- 2 *Definition of streamfunction*
- 3 *Taking the divergence of the definition equation of the streamfunction*
- 4 *Taking the divergence of the momentum equation 2.5*
- 5 *Making the equations from • 3 and • 4 dimensionless*
- 6 *Transformation of the equations from • 5 from a cartesian coordinate system to a general coordinate system*

The streamfunction ψ and the vorticity ω (both scalars), which are the variables in the governing equations, have the following definitions on a 2 D cartesian form :

Definition of vorticity

$$\omega = \nabla \times V \cdot k, \tag{2.6}$$

where the velocity vector $V = ui + vj$, and i, j are the unity vectors in the cartesian coordinate system.

Definition of streamfunction

$$V = -\nabla \times (\psi k) \tag{2.7}$$

or

$$u = -\frac{\partial \psi}{\partial y} \tag{2.8}$$

and

$$v = \frac{\partial \psi}{\partial x} \tag{2.9}$$

Taking the curl of the streamfunction equation (eq. 2.6) and applying the assumption of incompressibility of the flow (See eq. (2.7) - (2.9) leaves us with a Poisson equation on a cartesian form for the streamfunction :

$$\omega = -\nabla^2 \psi \tag{2.10}$$

Taking the divergence of the momentum equation 2.5

The vorticity transport equation on a cartesian form is obtained by taking the curl of the momentum equation (velocity transport equation) eq. (2.5). The matematical operations involved in deriving the vorticity equation for laminar flow is trivial and voluminious and left out here, but can be found in Appendix 8.1.

An incompressible, turbulent vorticity transport equation is then presented on the cartesian, 2 D and conservation form. After some rearrangements, as stated by [2] the second order derivatives of ν_τ[3]

can be isolated , and the following 2 equations is presented:

[3] ν_T is the dynamic turbulent viscosity or the turbulent diffusivity. For derivation, see section 2.4.3

$$\frac{\partial u\omega}{\partial x} + \frac{\partial v\omega}{\partial y} = \frac{\partial^2[\nu + \nu_\tau]\omega}{\partial x^2} + \frac{\partial^2[\nu + \nu_\tau]\omega}{\partial y^2} + \wp \qquad (2.11)$$

where

$$\wp = 2[\frac{\partial u}{\partial y}\frac{\partial^2 \nu_\tau}{\partial x^2} - (\frac{\partial u}{\partial x} - \frac{\partial v}{\partial y})\frac{\partial^2 \nu_\tau}{\partial x \partial y} + \frac{\partial v}{\partial x}\frac{\partial^2 \nu_\tau}{\partial y^2}] \qquad (2.12)$$

The second order derivatives of ν_T are collected in $\wp$ and may be neglected.

Dimensionless equations

The governing equations , the Poisson equation for the streamfunction 2.10 and the vorticity transport equation (eq. 2.11) are made dimensionless by introducing the dimensionless variables related to a characteristic length L_0 and a velocity V_0. The introduction of these dimensionless variables, which can be found in Appendix 8.2, do only alter the syntax of the *written equations* by replacing ν with Re_L and ν_T with Re_T in eq. (2.11) . For convenience we then express from now on the dimensionless variables with the same syntax, as we earlier used with respect to dimensioned variables.

2.3.1 Transformation from a cartesian to a general curvelinear coordinate system

In order to obtain proper definitions of the boundaries, which constitutes the geometrical shapes of bodies (airfoil etc.) and good representations of the spatial derivatives in the computational domain, the governing equations given in the cartesian coordinate system is transformed to a general curvelinear coordinate system.

The different differential operator terms (e.g. Laplacian term and convection term) which enter the governing equations on the cartesian form, (2.11) and (2.12), is replaced by similar transformed operators as part of the transformation.

The definition of the contra variant metric tensors g^{ij} , the jacobian J, the covariant velocities v^i and the differential operators applied in the transformation of the equations to a general coordinate u^i domain, and which enter the transformed governing equation eq. (2.13) and (2.14), is given in Appendix 8.1.

The final set of equations applied for discretization takes the form :

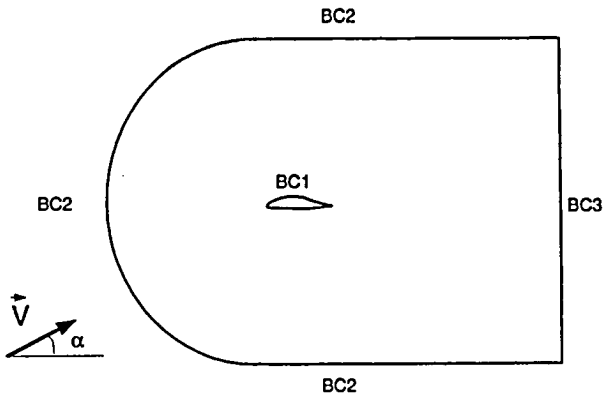

Figure 2.1: The physical domain for the flow around an airfoil with the corresponding boundary conditions.

$$\frac{1}{J}\frac{\partial}{\partial u^i}(Jg^{ij}\frac{\partial \psi}{\partial u^j}) = \omega, \qquad i \text{ and } j = 1,2 \tag{2.13}$$

$$\frac{\partial v^i \omega}{\partial u^i} - \frac{1}{JRe_l}\frac{\partial}{\partial u^i}(Jg^{ij}\frac{\partial[(1+\frac{Re_l}{Re_t})\omega]}{\partial u^j}) = 0 \tag{2.14}$$

2.3.2 Initial and boundary conditions for the governing equations

The governing equations are integrated in a pseudo time domain due to the applied ADI-scheme (Alternating Direct Implicit) described in chapter 3. This integration needs initial conditions and boundary conditions. The initial conditions and the boundary conditions for the steady flow around an airfoil are given below for the 2 governing equations.

Initial conditions

The initial conditions for the vorticity ω is simply given as zero in all of the domain.

The initial conditions for the streamfunction ψ is derived from the given uniform velocity field, with the velocity $\boldsymbol{V}$ having an angle α to the chord of the airfoil.

ψ is by definition linked to the covariant velocities v^1 and v^2 by :

$$-\frac{\partial \psi}{\partial \eta} = v^1 \tag{2.15}$$

$$\frac{\partial \psi}{\partial \zeta} = v^2 \tag{2.16}$$

where v^1 is the length of the covariant velocity tangential to the first general coordinate direction g_1 (u^1 or ζ) and v^2 is the lenght of the covariant velocity tangential to the second general coordinate direction g_2 (u^2 or η) and v^1 is related to the cartesian velocity $\boldsymbol{V}$:

$$v^1 = \boldsymbol{V} \cdot g_1 \tag{2.17}$$

Combining eq. (2.15) and eq. (2.17) leads to an integral equation for ψ (see e.g. fig. 2.1).

$$\psi(\eta) = \psi(\eta_{min}) + \int_{\eta_{min}}^{\eta} [V cos\alpha \frac{\partial x}{\partial \zeta} + V sin\alpha \frac{\partial y}{\partial \zeta}] d\eta \tag{2.18}$$

$\psi(\eta_{min})$ is set to zero at solid walls. At the rest of η_{min} $\psi(\eta_{min})$ is :

$$\psi(\eta_{min}) = V cos\alpha \frac{\partial x}{\partial \zeta} + V sin\alpha \frac{\partial y}{\partial \zeta} \tag{2.19}$$

Boundary conditions

The boundary conditions for the streamfunction ψ at the boundaries BC1 and BC2 is the Dirichlet type. They keep the same values as given under the initial conditions.

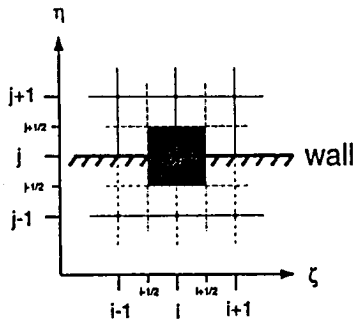

Figure 2.2: The control volume or cell approach applied to obtain the discrete equation for the vorticity ω at a solid wall.

BC1 - (ψ equation)

$$\psi \mid_{wall} = 0 \tag{2.20}$$

BC1 - (ω equation)

This boundary condition for ω is normally the weak spot in a ψ - ω formulation. In this finite difference formulation on conservation form, this wall boundary condition for ω is given on a finite volume form.

The Poisson equation for the streamfunction is applied as the boundary equation for the vorticity ω on solid walls e.g. a surface of an airfoil.

$$\omega \mid_{wall} = \nabla^2 \psi \mid_{wall} \tag{2.21}$$

Equation 2.21 can due to the finite volume formulation be expressed (in eq. 2.22 as a balance between the changes in the fluxes through a cell and the vorticity at the wall [4] :

[4] where e.g. *i+1/2* and *i-1/2* refers respectively to the forward and backward edge of the cell centered in (i,j) (in the ζ-direction) in the eq. (2.22), where it is recalled that $\nabla^2 = \nabla \cdot V = \frac{1}{J}\frac{\partial}{\partial u^i}(Jv^i) = \omega$

$$\omega_{ij}\mid_{wall} = -\frac{1}{J_{ij}}[(Jv^1)_{i+\frac{1}{2}} - (Jv^1)_{i-\frac{1}{2}} + (Jv^2)_{j+\frac{1}{2}} - (Jv^2)_{j-\frac{1}{2}}] \quad (2.22)$$

The 2 first terms in eq. (2.22) is zero because that the velocities are zero at the wall, and due to the continuity :

$$(Jv^2)_{j+\frac{1}{2}} = (Jv^2)_{j-\frac{1}{2}} \quad (2.23)$$

which changes 2.22 to the final discrete expression :

$$\omega_{ij}\mid_{wall} = \frac{2}{J_{ij}}(Jv^2)_{j+\frac{1}{2}} \quad (2.24)$$

or

$$\omega_{ij}\mid_{wall} = \frac{2}{J_{ij}}[(Jg^{21})\frac{\partial\psi}{\partial\zeta} + (Jg^{22})\frac{\partial\psi}{\partial\eta}]_{j+\frac{1}{2}} \quad (2.25)$$

BC2 - (ψ equation)

As stated elsewhere ψ keeps its initial value at this boundary.
BC2 - (ω equation)

$$\omega = 0 \quad (2.26)$$

BC3 - (ψ equation) At the far field boundary BC3 the curvature of the streamlines is assumed to be zero.

$$\frac{\partial^2\psi}{\partial\zeta^2} = 0 \quad (2.27)$$

BC3 - (ω equation)

A similar assumption on curvature are done for the vorticity at BC3.

$$\frac{\partial^2\omega}{\partial\zeta^2} = 0 \quad (2.28)$$

2.4 The turbulence model

To close the system of averaged Navier Stokes equations the Reynolds stresses appearing in these equations has to be modelled. In principal there exists 2 groups of models : 1st and 2nd order models. This work is concentrated on the branch of 1st order models termed zero equation or algebraic models.

2.4.1 1st order models

The common ground for the different 1st order models is that they take the same approach as the constitutive laws of an isotropic Newton-Stokes flow [43], when expressing the turbulent contribution to the stresses. This idea was first proposed by Boussinesq in 1877.

Because the operational range for the Mach number is assumed to be ≤ 0.5 for rotating wings and wing sections on windturbines we may apply the incompressible relation [2] :

$$\tau_{ij} + \frac{2}{3}\rho K\delta_{ij} = \rho\nu_T(\frac{\partial V_i}{\partial x_j} + \frac{\partial V_j}{\partial x_j}) \tag{2.29}$$

, where K is the turbulent kinetic energy and ν_T is the turbulent diffusivity. The first order closures are based on modelling this diffusivity.

The only difference between eq. (2.29) and the constitutive relations is that the latter links the flow stresses with a physical property of the fluid (the molecular diffusivity). The turbulent diffusivity is not a fluid property but a property of the flow.

For wall bounded flows the main velocity changes occurs in regions close to the wall, where experiments shows that the velocity distribution follows a universal logaritmic law (See fig. 2.3).

2.4.2 Algebraic turbulence models

The Baldwin-Lomax algebraic turbulence model was applied for several reasons. In general an algebraic model was chosen in favour of a two equation model (e.g. k-ϵ which are very common in engineering types of flows) because they are easy to implement, they can be in the order of 3 times as cheap as 2 equation models for 2 D flows [7] and they model the turbulence for attached airfoil flows with the same adequate accuracy as the latter for quite many airfoil types (See e.g. Cebeci and Smith 1974 [9], Baldwin and Lomax 1978 [3], Coakley 1983 [12], Cebeci et Al. 1986 [8], Lee and Pletcher 1986 [28], Kamiya 1990 [36], Baron 1992 [26]).

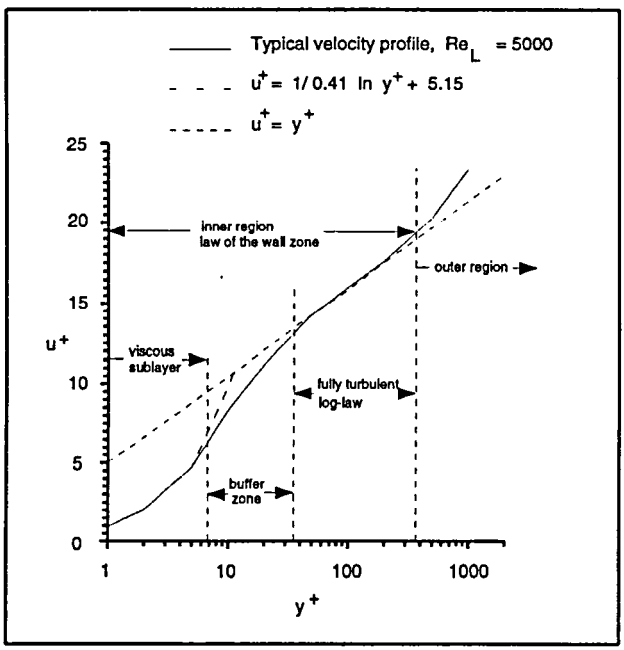

Figure 2.3: A typical velocity profile for the turbulent incompressible flow along a flat plate at $Re \simeq 5000$ compared with a three layer model for the boundary layer in the inner and outer region. The Baldwin-Lomax turbulence model is a 2 layer model, one for the inner zone and one for the outer.

Among the algebraic models applied on airfoils the Cebeci-Smith model [9] has been popular, and predicts well for the attached boundary layer flows, for which it was originally developed. The drawback for a zero equation model like the Cebeci Smith (CS)- model is that they predict the turbulence very poorly for separated flows. The reason for that is believed to be that the assumption on a local equilibrium between the production and dissipation of turbulent kinetic energy dosn't hold for separated flows. One need to account for history effects like convection and diffusion of turbulence.

But as discussed elsewhere the above mensioned effects, which are accounted for in 2 equation models has to be put into one parameter, the turbulent diffusivity ν_T represented in the Boussinesq relation, which again is multiplied by the gradient of the mean flow. This means that even 2 equation models predict the turbulent stresses under high influence of local parameters, and need not to be superiour to zero equation models.

The succes of the different models for different types of flows is also tightly connected to the election of the applied empiric coefficients in the models.

Even though the CS-model performs badly in separated flows, another algebraic model by Baldwin and Lomax [3] was applied in this work, because of the great advantage theese models represent with respect to numerical costs.

The BL-model which is based on the principles of the CS-model, has the advantage to the latter model, that the thickness of the boundary layer, which can be hard to find in separated flows or wakes, need not to be known.

As it will be treated in the following section the BL-model makes use of the vorticity, ω, of the flow which makes this turbulence model favorable for the applied averaged vorticity-streamfunction Navier-Stokes equations in comparence to a primitive variable approach, where the vorticity has to be found by extra computation.

2.4.3 The Baldwin-Lomax turbulence model

To suit the non dimensionalized averaged ω-ψ equations, the equations and characteristic parameters in the 2 layer Baldwin-Lomax turbulence model is put on a form applying the same expressions for nondimensionalization as was applied for the governing equations and which can be found in Appendix 8.2.

In the original paper from Baldwin and Lomax [3] expressions for the kinematic turbulent viscosity μ_T is given. This is suitable for compressible flows, where the effect of compressibility is entering the turbulence model by correcting the density ρ of the flow, which appear explicitly in the equations.

For the incompressible case, as we consider, applying the dynamic turbulent viscosity or turbulent diffusivity ν_T eliminates the density in the expressions and reduce the numerical cost.

The model consists of an inner, ν_{Ti}, and an outer, ν_{To} value for the turbulent diffusivity on the airfoil.

The wake region is modelled only by the outer value.

$$\nu_T = \left\{ \begin{array}{c} \nu_{Ti}, y < y_{crossover} \\ \nu_{To}, y_{crossover} < y \end{array} \right\}$$

The inner model consists of the Prandtl-Van Driest formulation, where the quantity in parenthesis in eq. (2.31) is the van Driest damping function, which bridge the gab between the fully turbulent region, where $l = \kappa\, y$ and the viscous sublayer, where $l \rightarrow 0$.

Some variations on the exponential function have been applied in order to account for effects of property variations so as pressure gradients, surface roughness etc. A discussion of modifications to account for several of these effects can be found in [9].

Frequently the van Driest constant A^+ is modified to account for complicating effects.

The length scale l which appear in the formula of the eddy viscosity coefficient ν_T should be evaluated along η - lines normal to the surface. As is the case in this work the grid generation is not always constructing grids, that are exactly normal to the surface. as quoted by Kayama [36] :"Those code and mesh dependencies rather than the physical model differences has significant effects on the numerical results of the flowfield in the present state of the art of N-S analysis."

$$\nu_{Ti} = l^2 |\omega| Re_l \tag{2.30}$$

where

$$l = \kappa y [1 - e^{\frac{-y^+}{A^+}}] \tag{2.31}$$

and

$$y^+ = \frac{u_\tau y}{\nu_w} Re_l \tag{2.32}$$

It appears reasonably clear from comparisons in the literature, that the inner layer model eq. (2.31) requires no modification to accurately predict the variable property flow of gases (e.g. air) with moderate pressure gradients on smooth surfaces [24].

The expression for the mixing length l (eq. 2.31) is responsible for producing the inner "Law-of-wall" (see fig. 2.3) region in turbulent flow.

The outer formulation take the form :

$$\nu_{To} = KC_{CP}F_{WAKE}F_{KLEB} \tag{2.33}$$

where

$$F_{WAKE} = \left\{ \begin{array}{c} y_{Max}F_{Max} \\ or \\ C_{WK}y_{Max}V_{DIF}^2 \end{array} \right\} \quad ,the\ smaller$$

y_{Max} and F_{Max} is determined from the function

$$F(y) = y|\omega|[1 - e^{\frac{-y^+}{A^+}}] \tag{2.34}$$

In the wake region $e^{\frac{-y^+}{A^+}}$ is set to zero. F_{MAX} is the maximum value of the F(y) function, and y_{Max} is the value of y, where it occur.

The Klebanoff intermittency factor[5] is given by

$$F_{KLEB}(y) = [1 + 5.5(\frac{C_{KLEB}y}{y_{Max}})^6]^{-1} \tag{2.35}$$

V_{DIF} is the difference between maximum and minimum total velocity in a profile (at a fixed x-station) and is

$$V_{DIF} = (\sqrt{u^2 + v^2})_{Max} - (\sqrt{u^2 + v^2})_{Min} \tag{2.36}$$

the second term in eq. (2.36) is zero except for the wake region.

The length scale l which appear in the formula of the eddy viscosity coefficient ν_T should be evaluated along η - lines normal to the surface. As is the case in this work the grid generation (see Appendix A3) is not always constructing grids, that are exactly normal to the surface. The evaluation of l has some ambiguity in its definition. It is not rigorously defined and therefore is dependent on how the numerical describtion, programming and grid distributions is used by individuel investigators. As quoted by Kamiya [36] :"Those code and mesh dependencies rather than the physical model differences has significant effects on the numerical results of the flowfield in the present state of the art of N-S analysis."

Kamiya [36] recommend to investigate this matter in a future work, and in the following section the author made some investigations and gives recommandations in order to make it easy to construct prober grids for application with the Baldwin - Lomax turbulence model.

[5]"At a certain range of Reynolds numbers, around the critical, the flow becomes *intermittent*, which means that it alternates in time between being laminar or turbulent. the intermittency factor, is defined as the fraction of time during which the flow at a given position remains turbulent". [43]

2.4.4 Guidelines for grid construction in relation to Baldwin-Lomax turbulence modelling

Ranges for y_2^+

The algebraic turbulence models as Cebeci-Smith and Baldwin-Lomax, which are modelling the turbulent diffusivity including the laminar sublayer, is known to break down if y_2^+ (See fig. 2.4) becomes sufficient small ($y_2^+ \ll 1$) [10]. On the other hand, experience shows that if y_2^+ is to big a converged solution cannot be obtained. The author made a serie of tests for different Reynolds numbers in the range of 1-3 million and incidences in the range of 0^o - 16^o for a NACA0012 and a NTUA airfoil. The tests showed that if $1 < y_2^+ < 5$ converged solution were obtained in al cases. For higher values of y_2^+ few converged solutions were obtained.

Because $y^+ = y^+(u_\tau)$ and u_τ is part of the flow solution, constructing a grid for Baldwin-Lomax turbulence modelling is adaptive in some way. Sofisticated adaptive grid construction models has been proposed Kallinderis et Al. [26] and applied [23], but the author found that some hand rules could be extracted from grid construction tests, with a simple hyperbolic grid generator, for different airfoils, Reynolds numbers and incidences. These hand rules makes it easy to assure that converged solutions easily can be obtained.

Gradients in ν_τ at the trailing edge

To avoid to high gradients in ν_τ at the trailing edge (and a corresponding low depth of convergence) the grid cell length on the trailing edge is chosen to be $\Delta\zeta = 0.01C$ for all airfoil flow calculations in the Reynolds number range 1 - 3 million. The grid is constructed by a simpel hyperbolic grid generator with 230-260 gridpoints in the $\zeta - direction$ (170-200 on the airfoil) and 51 in the $\eta - direction$.

Experiences in grid construction, by applying a simple hyperbolic grid generator, shows that a handrule can be extracted for finding the grid distance between the airfoil (NACA0012) and the 1st gridpoint in the normal direction at the trailing edge of a grid applied for attached flows, $\Delta\eta_{y_2^+=Constant}\,|_{t.e.}$ (see e.g. fig. (2.4)).

$$\Delta\eta_{y_2^+=Constant}\,|_{t.e.} \sim Re_l \tag{2.37}$$

For Re = 10^6 :

$$\Delta\eta_{y_2^+=5}\,|_{t.e.} \simeq 5.0 \cdot 10^{-5} \tag{2.38}$$

and for Re = $2 \cdot 10^6$

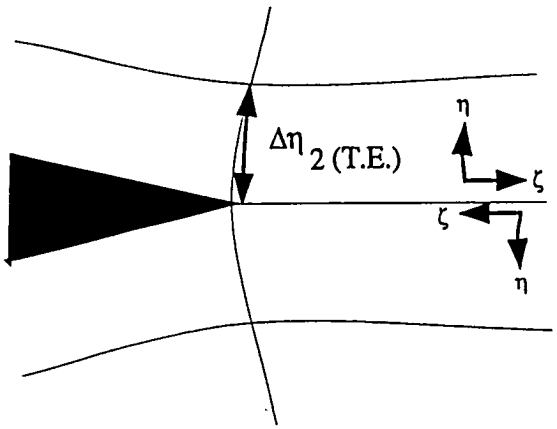

Figure 2.4: The grid distance $\Delta\eta_2$ in the grid at the trailing edge corresponding to y_2^+.

$$\Delta\eta_{y_2^+=5}\,|_{t.e.} \simeq 2.5 \cdot 10^{-5} \tag{2.39}$$

The distance $\Delta\eta_{y_2^+=5}\,|_{t.e.}$ for $Re = 10^6$ is also applied by [36] for an equal flow situation.

The upwind scheme (see section 5.1) and the grid distribution add numerical diffusivity, which are locally bounded to the grid and in a way can be seen as a kind of volume forces. This makes it difficult to interpret the flow situation in a physical way, because e.g. the total set of shear forces consists of a global component related to the molecular diffusivity, and two local components, respectively turbulent and numerical diffusivity.

2.5 The Formulation of the pressure equation

The determination of the pressure is done in a subsequent step when the streamfunction and vorticity field is known. An extra equation has to be solved.

Normally this equation is obtained by taking the divergence of the momentum equation 2.5 and becomes :

$$-\frac{1}{\rho}\nabla^2 p = \nabla\cdot(\nabla\cdot\nabla V) \tag{2.40}$$

Often this equation is solved with Neumann boundary conditions along solid walls (BC1 at fig. (2.1)).

$$\frac{\partial p}{\partial n} = 0 \tag{2.41}$$

and p = 0 at the farfield boundary (BC2 and BC3 at fig. (2.1).

The major drawback associated with the previous equation is the fact that the accuracy with which this equation is solved is directly related to the accuracy that the right hand side (RHS) is calculated. Local inaccuracies in calculating the second order derivatives appearing in the RHS term, may restrict the convergence depth of the equation, due to the integral constraint, (Greens theorem) which needs to be globally satisfied.

To avoid this problem a new pressure formulation is proposed by P. Chaviaropoulous et Al. [37] which is based on a stagnation pressure transport equation. The derivation of the following applied equation for the static pressure, p_t, can be found in Appendix A4 :

$$\rho V\cdot\nabla p_t - \frac{1}{Re}\nabla^2 p_t = -\frac{1}{Re}\rho\omega^2 \tag{2.42}$$

where the static pressure, p_t, is related to the total pressure, p, through the steady Bernoulli equation :

$$p = p_t - \frac{1}{2}\rho V^2 \tag{2.43}$$

In equation 2.42 the RHS term is easy to compute accurately, being a simple function of the vorticity, which is one of the independent variables in the present $\psi - \omega$ formulation.

2.5.1 Boundary conditions for the pressure equation

A Neumann boundary condition for the stagnation pressure may be provided by projecting eq. (8.48) on to the direction normal to the boundary.

For solid walls the no-slip condition simplifies the equation and results in :

$$\frac{\partial p_t}{\partial n} = \frac{1}{Re}\frac{\partial \omega}{\partial s} \tag{2.44}$$

where n is the normal direction to the wall and (s) the tangential.

The Neumann boundary condition for total pressure is, unlike the commonly used for static pressure, directly related to the first derivatives of the independent variable ω matching the accuracy of the previous derived pressure equation.

At the farfield boundary the static pressure is set to zero.

Chapter 3

Solution of the governing equations

The governing equation is solved using the following techniques:

- 1. Conservative formulation of the governing equations.
- 2. Newton linearisation.
- 3. Approximated factorization - ADI.
- 4. GMRES.

3.1 The numerical integration scheme

3.1.1 The conservative form

The governing equations, as they are given in eq. (2.13) and eq. (2.14), are on a strong conservation or divergence form, which matematically means that the coefficients are either constants or, if variable, their variables appear no where in the equations. Seen from a physically point of view this divergence form is suitable for equations representing conservation of a physical property like e.g. mass or momentum in respectively eq. (2.13) and eq. (2.14).

The advantage of the conservation form of Partial Differential Equations (PDE) can be illustrated by the continuity equation

$$\nabla \cdot \rho V = 0 \tag{3.1}$$

Let eq. (3.1) be approximated by a suitable[1] finite difference representation.

For an arbitrary control volume, which include the entire problem domain or any fraction of it, conservation of mass for steady flows requires that the net mass flux be zero (the mass flow rate *in* equals the mass flow rate *out*).

This can be observed formally by applying the divergence theorem to the governing equations (here represented by the continuity equation)

$$\int\int\int_R \nabla\cdot\rho V dR = \int\int_S \rho V\cdot\vec{n} dS = 0 \tag{3.2}$$

To see if this finite difference representation eq. (3.1) has the conservative property, it must be established that the discretized version of the divergence theorem is satisfied. One can e.g. check this for a control volume consisting of the entire flow domain.

To do this the integral on the left is evaluated by summing the difference representation of eq. (3.1) at all grid points. If the difference scheme has the conservative property, all terms will cancel except those which represent fluxes at the boundaries.

It should be possible to rearrange the remaining terms to obtain identically a finite difference representation of the integral on the right. For this example the result of the integration will be a verification, that the mass flux into the control volume equals the mass flow out.

If the difference scheme used for the PDE is not conservative, the numerical solution may permit the existence of small mass sources or sinks, this is the case for a non conservative scheme.

Schemes having the conservative property occur in a natural way when differencing starts with the divergence form of the PDE.

3.1.2 Newton linearization

The numerical integration of the kinematic field eq. (2.11) and eq. (2.12) is obtained in a strongly coupled mode using a Newton iterative scheme. In other words, the variable ω appears at the same timestep n in both of the governing equations, when solved. Let $\boldsymbol{f} = (\psi, \omega)^T$ be the vector of the independent variables and $\mathbf{R}$ the residual vector which, at the n^{th} iteration, may be written on a form [37]:

[1]This finite difference scheme shall be *consistent*, which means that for $\Delta x \to 0$ the difference between the solution to the real PDE and the discretized one shall approach 0. This is illustrated best considering a non consistent scheme like the Dufort-Frankel scheme, which can be found in [24]

$$R^n = \begin{bmatrix} A_{11} & 1 \\ 0 & A_{22} \end{bmatrix}^n f^n = \tag{3.3}$$

$$\begin{bmatrix} \frac{1}{J}\frac{\partial}{\partial u^i}(Jg^{ij}\frac{\partial[]}{\partial u^j}) & I \\ 0 & \frac{\partial v^i[]}{\partial u^i} - \frac{1}{JRe_l}\frac{\partial}{\partial u^i}(Jg^{ij}\frac{\partial[(1+\frac{n_{e_l}}{Re_l})[]]}{\partial u^j}) \end{bmatrix} f^n$$

, where the superscript (n) denotes the iteration level. A_{11} and A_{22} is matrix elements and operator equations.

A step of the Newton iteration is formed as :

$$R^{n+1} = R^n + \underline{(\frac{\partial R}{\partial f})}^n \Delta f = 0 \tag{3.4}$$

where

$$f^{n+1} = f^n + \Delta f \tag{3.5}$$

and the Jacobian matrix

$$\underline{(\frac{\partial R}{\partial f})}^n = \begin{bmatrix} A_{11} & 1 \\ 0 & A_{22} \end{bmatrix}$$

is linearized only with respect to the operator A_{22}, which includes the convection term $\nabla[V()]$, while A_{11} is a pure linear operator.

The linearized system of equations 3.3 is left preconditioned by an approximate matrix $\underline{P}^n$. The preconditioning will if requested[2] rearrange a "near" singular matrix, with a bad distribution of the coefficients in the matrix, so they are more uniformly distributed, and thereby an iterative inversion of the matrix will have a significant higher convergence rate, and the solution will be more accurate.

As shown in the paper by [48] preconditioning is necessary to get an acceptable computing time.

An obvious choice[3] of a preconditioning matrix is

$$\underline{P}^n \simeq \left[(\frac{\partial R}{\partial f})^n\right]^{-1} = \begin{bmatrix} A_{11}^{-1} & -A_{11}^{-1}A_{22}^{-1} \\ 0 & A_{22}^{-1} \end{bmatrix}$$

The reason for the approximated relation between the preconditioning matrix on the left side of eq. (3.1.2), $\underline{P}^n$, and the matrix containing

[2]E.g. for high Reynolds number flows, with high gradients in the grid distribution, this is likely to be the case for the Jacobian matrix.

[3]In order to find a matrix product close to a unity matrix.

inverted elements of the matrix $\underline{A}$ from eq. (3.3), on the right hand side, is that the matrix elements in $\underline{P}$, due to the applied ADI scheme, contains inverted and factorized elements of matrix $\underline{A}$.

The ADI scheme and the factorization of the preconditioning matrix $\underline{P}$ is described in the following section.

3.1.3 The ADI technique

The diagonal submatrices of the Jacobian matrix are approximately factorized using an ADI (Alternating Direct Implicit) technique in order to facilitate its inversion.

The preconditioning matrix $\underline{P}^n$ (See e.g. Appendix 8.6) can be written :

$$\underline{P}^n = \begin{bmatrix} P_{11}^{-1} & -P_{11}^{-1}P_{22}^{-1} \\ 0 & P_{22}^{-1} \end{bmatrix} \tag{3.6}$$

where

$$P_{11} = -\frac{1}{\Delta t_\psi}\{I - \frac{\Delta t_\psi}{J}(Jg^{11}\frac{\partial}{\partial \zeta}())\}\{I - \frac{\Delta t_\psi}{J}(Jg^{22}\frac{\partial}{\partial \eta}())\} \tag{3.7}$$

and

$$P_{22} = -\frac{1}{\Delta t_\omega}\{I + \Delta t_\omega(\frac{\partial}{\partial \zeta}[()v^1] - \frac{1}{JRe_l}\frac{\partial}{\partial \zeta}(Jg^{11}\frac{\partial}{\partial \zeta}([1 + \frac{Re_l}{Re_T}]()))\}$$
$$\{I + \Delta t_\omega(\frac{\partial}{\partial \eta}[()v^2] - \frac{1}{JRe_l}\frac{\partial}{\partial \eta}(Jg^{22}\frac{\partial}{\partial \eta}([1 + \frac{Re_l}{Re_T}]()))\} \tag{3.8}$$

Δt_ψ is a pseudo time step for the ψ- equation, and Δt_ω is a pseudo time step for the ω-equation.

The left preconditioning of equation (3.3) yields

$$\boldsymbol{R}^* + \underline{D}\Delta \boldsymbol{f} = 0 \tag{3.9}$$

where

$$\boldsymbol{R}^* = (\underline{P}\boldsymbol{R})^n, \underline{D} = [\underline{P}(\frac{\partial R}{\partial f})]^n \simeq \underline{I} \tag{3.10}$$

Because $\underline{D} \simeq \underline{I}$ eq. (3.9) can give the updated values for $\boldsymbol{f}$ using the approximation $\Delta \boldsymbol{f} = -\boldsymbol{R}^*$.

This algorithm constitutes a revised fully implicit $\psi - \omega$ solver on a factorized ADI basis, that handles the stream-function equation in a fully implicit mode for both ψ and ω variables, taking into account the non-diagonal term of the Jacobian matrix.

ADI and periodic boundaries

Finding the solution to the governing flow equations on e.g. an O-grid or a C-grid introduces a periodic boundary (PB) in the computational domain.

There exists at least 3 techniques with increasing complexity to handle a PB.

1) The simplest technique is to let the derivatives at the periodic boundary (those perpendicular to the PB), which, on it's discrete form have variables that relates to the other side of the PB, be at a previous time step in the ADI- solver.

An example refering to fig. 3.1 could be e.g. a second order derivative [4]:

$$\frac{\partial^2 \psi}{\partial \eta^2} \Big|_{i,1}^{n+1} = \frac{\psi_{i,2}^{n+1} - 2 \cdot \psi_{i,1}^{n+1} + \psi_{ii,2}^{n}}{(\Delta\eta)^2} + O(\Delta\eta)^2 \qquad (3.11)$$

This technique preserves the three-diagonality of the matrices, an thereby a fast inversion of the matrices and a numerical solution by ADI.

2) There exists a second technique for C-grids where the PB is removed in relation to the ADI-solver. By putting the 2 smaller tridiagonal matrices from respec tively the upper an lower side of the PB (when line-solving perpendicular to the PB) in the wakezone into one big tridiagonal matrice all points in the computational domain is correctly updated (See fig. 3.2).

The only disadvantages of this technique is the extra numerical cost related to copying between small and big matrices.

3) A third technique make a correct updating in all points in the computational domain but the PB gives raise to off-diagonal elements in the ADI factorized tridiagonal matrices. To save the extra numerical expences related to transfering of variables between the different arrays as in 2), additional programming must be done in order to change a standard line solver, to account for these off diagonal elements.

For the laminar and turbulent airfoil flows modelled on a C-grid there is a coincidence between the physical location of large gradients in vorticity and streamfunction in the wake region and the location of the periodic boundary. For the turbulent case, additionally this is also the case for the turbulent viscosity ν_T.

In order to quantify how much the convergence rate is affected by respectively applying "update-technique" no. 1 or 2, two codes, one based on each technique were developed. In fig. 3.3 the convergence rates for the two techniques are compared. The comparison is done for a flow around a NACA 0012 at a Reynolds numbers of 1000 and an incidence of 5°.

[4] Where i refers to the domain below the PB (low number of i) and ii refers to the

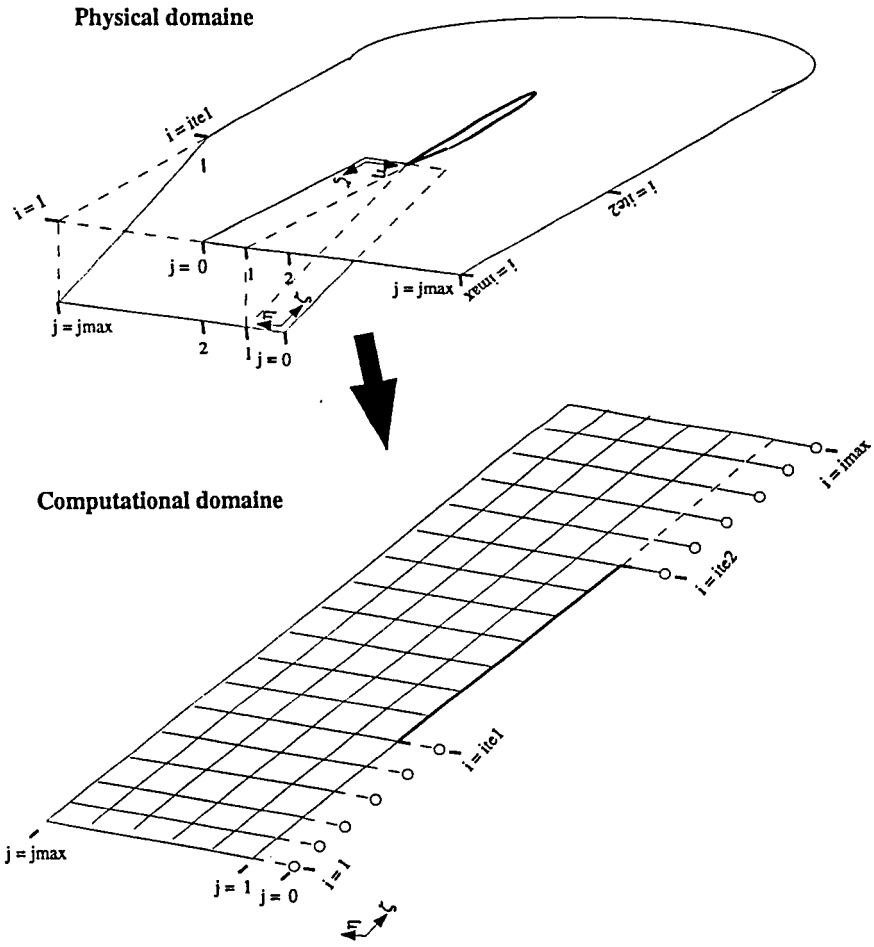

Figure 3.1: When evaluating e.g. a second order derivative, on the upper side of the periodic boundary (j = 1) for a C - grid, the variables (e.g. ψ) related to the lower side is given at a previous timestep, for update technique no. 1. For update technique no. 2 and 3 all variables are given at the same time step.

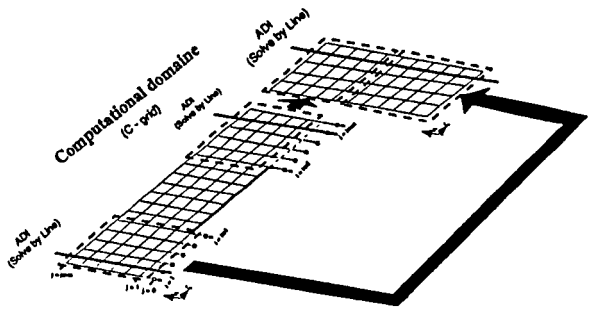

Figure 3.2: One of the techniques to handle the periodic boundary (PB) for a C-grid is illustrated. The PB is eliminated by transfering the variables from 2 "small" arrays, representing the grid points in the upper and lower wake zone, into 1 "big" array, before applying the ADI line solver.

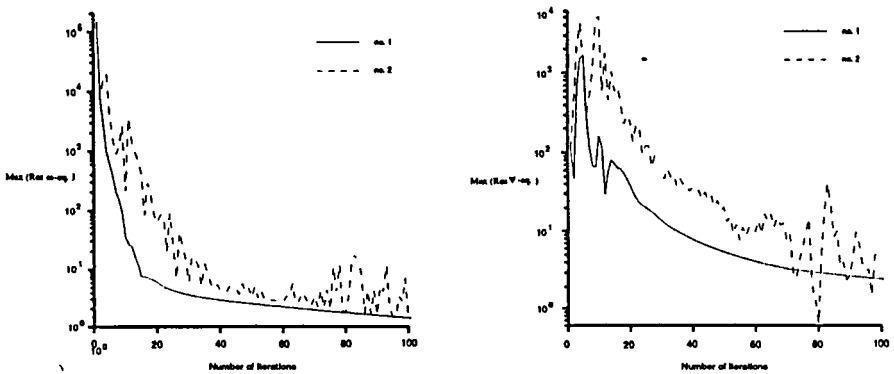

Figure 3.3: Convergence rate for the maximum residual in the flow domain for respectively a) the vorticity equation and b) the streamfunction equation. In each figure the number 1 and number 2 update technique for the periodic boundary is compared.

From figur 3.3 it is seen that for this steady laminar flow around a NACA 0012 airfoil the update technique number 1 has the best convergence rate. It is recalled that this technique is the numerically cheapest per iteration, and further it apply the simplest programming technique.

3.1.4 GMRES - Generalized Minimal Residual method

In order to reduce the dependence of convergence on the choice of pseudo timestep and to increase the convergence rate of the solver, there was introduced a further improvement in the numerical integration scheme. This improvement was achieved by solving the system of equations (3.9) in it's original form (by retaining the D matrix) using the restarting linear GMRES [42] scheme.

The GMRES scheme (see appendix 8.5) works as a relaxation scheme in the sence that it determines "relaxation" parameters α which are applied in the iteration proces when the streamfunction ψ and the vorticity ω are updated. That is, as part of the Newton linearization eq. (3.5) is relaxed.

$$f^{n+1} = f^n + \alpha \Delta f \tag{3.12}$$

Additionally the vorticity and streamfunction boundary conditions may easily be implemented in the restarting GMRES scheme because of their linear nature. This scheme has proven to be very effective in a variety of CFD problems [37].

The GMRES method and number of Krylov subspaces.

To find an optimum for the smallest numerical cost P. Chaviaropoulous et Al. [37] made a test for a Driven Cavity at different Reynolds numbers, with different pseudo time steps and applying different numbers of Krylov Subspaces (KS's). Because the application of different numbers of KS's in itself changes the applied time for running one total iteration cycle, the reduction in residuals has to be compared with the total employed CPU time.

One conclusion was that the highest gains in reduction of residuals compared to total employed CPU - time was stepping from 1 to 3 KS's, but still 6 KS's performs a little better. Tests made by P. Chaviaropoulous et Al. [37] showed that applying 7 or 10 KS's didn't make much difference on the convergence rate, and to limit the applied memory a maximum limit of 10 KS' can be used in the code.

For all turbulent airfoil computations 7 Krylov Subspaces were used.

---

domain above the PB.

Another conclusion was that even though the dependence of the choice of pseudo time step is reduced, there is still room for improving the efficiency of this code by finding optimal series of time steps.

A straight forward solution could be to apply the Wachpress time step optimization routine [49], which, with succes, has been applied by [22].

But the overall conclusion for e.g. laminar flows around airfoils is that The Newton linearization with the ADI precondition matrices together with the GMRES method constitutes an efficient solution method.

Chapter 4

Solution of the pressure equation

A simpler numerical integration technique is adopted for the solution of the transport equation for the stagnation pressure field (2.42), once the kinematic field is known. The applied scheme is an approximate factorization iterative one of ADI type which reads :

$$\Delta p_t = -P_{22}^{-1} R_{p_t} \tag{4.1}$$

$$p_t^{n+1} = p_t^n + \Delta p_t \tag{4.2}$$

Where R_{p_t} is the stagnation pressure equation residual and P_{22} the convection-diffusion operator approximation introduced in equation (2.42).

The inversion of P_{11} and P_{22} is a straightforward task requiring the inversion of four tridiagonal matrices for each Newton iteration. The ADI preconditioner was preferred among others (for example incomplete LU decomposition) because of its minimum computer storage requirements and its easy implementation on vector/parallel machines.

Chapter 5

The discretized equations

The governing equations on conservation form are discretized in the following way, refering to fig. 5.1 :

Laplacian operator on ψ- and ω- equation

$$\nabla^2() \mid_{(i,j)} = \frac{1}{J_{(i,j)}}[\frac{\partial()}{\partial u^1}([Jg^{11}\frac{\partial()}{\partial u^1}]+[Jg^{12}\frac{\partial()}{\partial u^2}])+\frac{\partial()}{\partial u^2}([Jg^{21}\frac{\partial()}{\partial u^1}]+[Jg^{22}\frac{\partial()}{\partial u^2}])] \tag{5.1}$$

The outer operators discretized gives :

$$\nabla^2() \mid_{(i,j)} = \frac{1}{J_{(i,j)}}[([Jg^{11}\frac{\partial()}{\partial u^1}]+[Jg^{12}\frac{\partial()}{\partial u^2}])_{i+1/2,j}-([Jg^{11}\frac{\partial()}{\partial u^1}]+[Jg^{12}\frac{\partial()}{\partial u^2}])_{i-1/2,j} \tag{5.2}$$

$$+([Jg^{21}\frac{\partial()}{\partial u^1}]+[Jg^{22}\frac{\partial()}{\partial u^2}])_{i,j+1/2}-([Jg^{21}\frac{\partial()}{\partial u^1}]+[Jg^{22}\frac{\partial()}{\partial u^2}])_{i,j-1/2}] \tag{5.3}$$

where the inner derivatives are :

$$\frac{\partial()}{\partial u^1} \mid_{i+1/2,j} = ()_{i+1,j} - ()_{i,j} \tag{5.4}$$

and

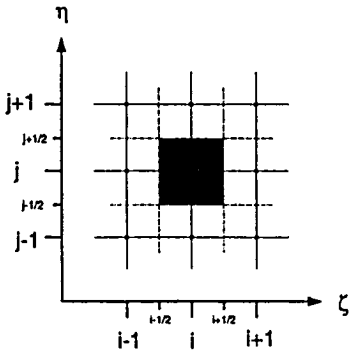

Figure 5.1: The discretization stencil applied for the governing equations on the conservation form.

$$\frac{\partial()}{\partial u^2}\,|_{i+1/2,j} = 0.25[()_{i+1,j+1} + ()_{i,j+1} - ()_{i+1,j-1} - ()_{i,j-1}] \tag{5.5}$$

The approximation of the metric-coefficients are governed by the discretization of the related derivatives, e.g. :

$$[Jg^{11}]_{i+1/2}[\frac{\partial()}{\partial u^1}]_{i+1/2,j} = 0.5[(Jg^{11})_{i+1,j} + (Jg^{11})_{i,j}][()_{i+1,j} - ()_{i,j}] \tag{5.6}$$

and

$$[Jg^{12}]_{i+1/2}[\frac{\partial()}{\partial u^2}]_{i+1/2,j} = 0.25[(Jg^{12})_{i+1,j+1} + (Jg^{12})_{i,j+1} \tag{5.7}$$

$$- (Jg^{12})_{i+1,j-1} - (Jg^{12})_{i,j-1}]0.25[()_{i+1,j+1} + ()_{i,j+1} - ()_{i+1,j-1} - ()_{i,j-1}] \tag{5.8}$$

In a similar manner the other derivatives and metric coefficients are discretized.

Convective operator on the ω- equation

The convective term in the ω- equation is on the conservative form. To secure that the matrices related to the vorticity transport equation are

diagonal dominant and thereby unconditionally stable, a first order upwind scheme is applied.

$$\nabla \cdot (U\omega) \mid_{(i,j)} = \frac{1}{J_{(i,j)}}[\frac{\partial()}{\partial u^1}(J\omega v^1) + \frac{1}{J}\frac{\partial()}{\partial u^2}(J\omega v^2)]_{(i,j)} = \tag{5.9}$$

$$\frac{1}{J_{(i,j)}}[(J\omega v^1)_{i+1/2,j} - (J\omega v^1)_{i-1/2,j}] + \frac{1}{J_{(i,j)}}[(J\omega v^2)_{i,j+1/2} - (J\omega v^2)_{i,j-1/2}] \tag{5.10}$$

Where the first order upwind is introduced as :

$$(J\omega v^1)_{i+1/2,j} = \omega_{i,j} MAX[(Jv^1)_{i+1/2,j}; 0] - \omega_{i+1,j} MAX[(-Jv^1)_{i+1/2,j}; 0] \tag{5.11}$$

$$(J\omega v^1)_{i-1/2,j} = \omega_{i-1,j} MAX[(Jv^1)_{i-1/2,j}; 0] - \omega_{i,j} MAX[(-Jv^1)_{i-1/2,j}; 0] \tag{5.12}$$

$$(J\omega v^2)_{i,j+1/2} = \omega_{i,j} MAX[(Jv^2)_{i,j+1/2}; 0] - \omega_{i,j+1} MAX[(-Jv^2)_{i,j+1/2}; 0] \tag{5.13}$$

$$(J\omega v^2)_{i,j-1/2} = \omega_{i,j-1} MAX[(Jv^2)_{i,j-1/2}; 0] - \omega_{i,j} MAX[(-Jv^2)_{i,j-1/2}; 0] \tag{5.14}$$

5.1 2nd order upwind schemes

To obtain a better approximation of the convective term a second order scheme, - the QUICK (Quadratic Upstream Interpolations for the Convective Kinematics) scheme proposed by e.g. Leonard 1979 is applied. The idea of using this scheme is to be more accurate like a Central Difference (CD) scheme but more stable like a first order scheme.

This method fits the contra variant velocities on the interface of a cell by a second order polynomial.

$$v_e^i = v_P^i + S_e; S_e = \frac{1}{8}(3v_E^i - 2v_P^i - v_W^i if U_e > 0 \tag{5.15}$$

$$v_e^i = v_E^i + S_e; S_e = \frac{1}{8}(3v_P^i - 2v_E^i - v_{EE}^i if U_e < 0 \tag{5.16}$$

$$v_w^i = v_W^i + S_w; S_w = \frac{1}{8}(3v_P^i - 2v_W^i - v_{WW}^i if U_e > 0 \tag{5.17}$$

$$v_w^i = v_P^i + S_w; S_w = \frac{1}{8}(3v_W^i - 2v_P^i - v_E^i if U_e < 0 \tag{5.18}$$

The QUICK scheme, depending on the method of implementation may yield coefficients which becomes negative and leads to convergence problems. To obtain convergence the scheme must be recast into a diagonally dominant form, where the source term, due to the QUICK scheme is sufficiently small, and according to [41], will not hinder convergence significantly.

For the high Reynolds number (turbulent) flows around airfoils the convergence rate are disimproved so badly, that the QUICK scheme is not applied here.

Chapter 6

Computational solutions to the system of governing flow equations

The numerical scheme previous described has been tested on two types of flows steady laminar and steady turbulent flow.

6.1 Solutions for steady laminar cases

The steady laminar test cases limits themselves to computations of the flow around a cylinder at different Reynolds numbers and to computations on A NACA0012 airfoil.

6.1.1 Flow around a cylinder at Re = 5, 7, 10, 20 and 40

The numerical scheme is firstly tested by modelling the steady laminar flow around a cylinder at Reynolds numbers of 5, 7, 10, 20 and 40. The computations were done on the C - grid shown in fig. 6.1 and the results were compared to Chang and Dennis [13], who also applied a vorticity - streamfunction formulation.

The convective terms in the vorticity transport equation were modelled by a second order central scheme, because this scheme, at these low Reynolds numbers, are numerical stable and more accurate than a first order upwind scheme, applied for computations at high Reynolds numbers.

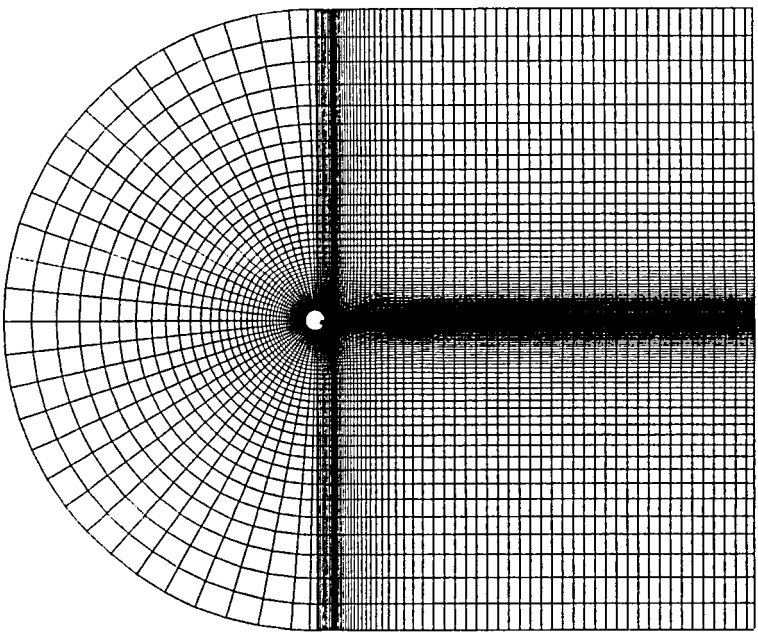

Figure 6.1: C-grid around cylinder.

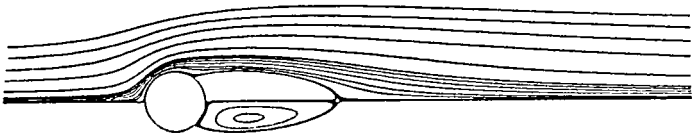

Figure 6.2: Streamlines for the flow around a cylinder at Re = 20.

In fig. 6.2 the streamlines and recirculation zone for the flow around the cylinder, at a Reynolds number of 20, can be seen.

Chang and Dennis [13] made computations of the pressure - and vorticity distribution on the surface of the cylinder and in respectively fig. 6.3 and 6.4 similar obtained results are compared. There is a good agreement between the present results and those given by Chang and Dennis. The largest differences in the distribution of surface pressure and vorticity occur behind the cylinder in the recirculation zone and is caused by a bad grid in this zone. When constructing the C-grid around the cylinder, the grid cells behind the cylinder becomes the less orthogonal in the whole grid.

Normally an O-grid would be applied for the calculation of the flow around a cylinder giving a homogeneous quality and orthogonal cells in the entire grid.

For the different Reynolds numbers present calculations of characteristic parameters like : the length of the recirculation zone L, the angle of separation Θ_s, the total friction coefficient C_F, the total pressure coefficient C_P and the drag coefficient C_D is compared to Chang and Dennis [13]. The results are given in fig. 6.5 and the second row in the table represents the present calculations.

6.1.2 Flow around a NACA 0012 airfoil at $\alpha = 5^o$ and Re = 1.000

In fig. 6.6 the streamlines for the flow around a NACA0012 airfoil, is compared for respectively a solution where the first order upwind scheme and a second order central scheme has been applied for the convective terms. The characteristic difference in the size of the recirculation zones is noticed. The first order upwind scheme introduce numerical diffussion and the effective Reynolds number is lowered, resulting in the smaller recirculation zone.

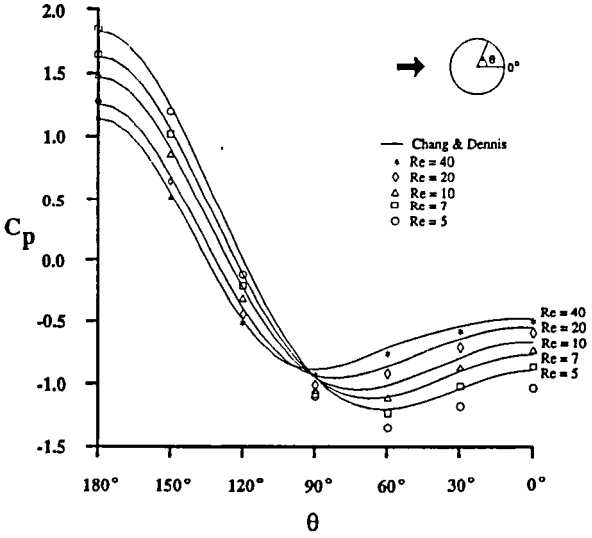

Figure 6.3: Pressure coefficient on surface of cylinder.

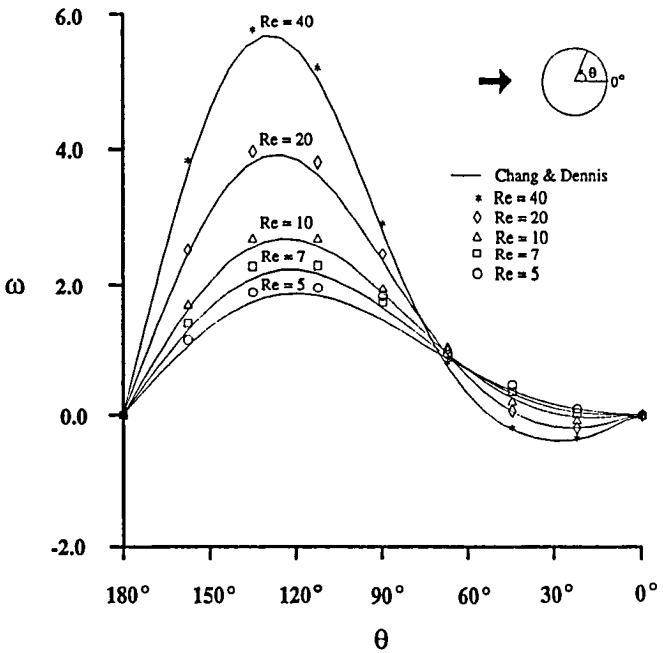

Figure 6.4: Vorticity on surface of cylinder.

Re	L	θ_s	C_F	C_P	C_D
5	-	-	1.917	2.199	4.116
	-	-	1.810	2.060	3.870
7	0.19	15.9	1.553	1.868	3.421
	-	-	1.480	1.770	3.250
10	0.53	29.6	1.246	1.600	2.846
	0.43	24.7	1.190	1.530	2.730
20	1.88	43.7	0.812	1.233	2.045
	1.84	32.7	0.790	1.190	1.980
40	4.69	53.8	0.524	0.998	1.522
	4.59	38.1	0.510	0.970	1.480

Figure 6.5: Tabel giving the relation between the Reynolds number, Re, and the length of the recirculation zone, L, the angle of separation, Θ_s, the total friction coefficient, C_F, The total pressure coefficient, C_P and the drag coefficient C_D for the flow around a cylinder.

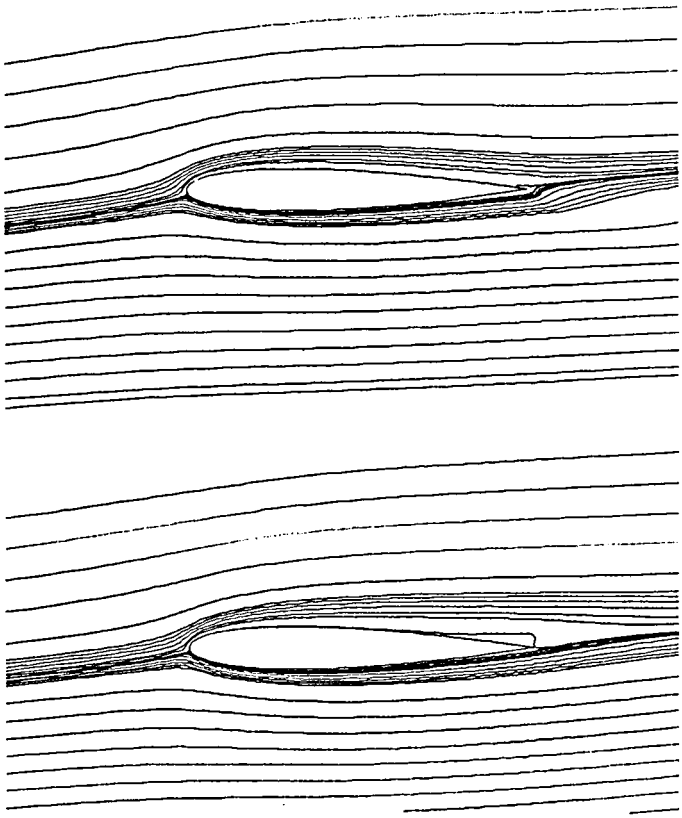

Figure 6.6: Streamlines for flow around a NACA0012 airfoil for Re = 1000 and $\alpha = 5°$. a) First order upwind scheme. b) Second order central scheme.

6.2 Solutions for steady turbulent cases

The numerical scheme including the Baldwin - Lomax turbulence model is firstly testet on a symmetrical NACA0012 airfoil. The turbulence model does not include any transition model, which means that transition at a point must be set manually. For the calculations presented here for airfoils, leading edge transition has been applied.

6.2.1 Flow around a NACA0012 airfoil at $\alpha = 0^o$ and $\mathrm{Re} = 10^6$

A typical grid used for the calculations of flows around the NACA0012 airfoil is shown in fig. 6.7 having 231 x 51 grid points. As concluded earlier the applied grids has a big influence on the accuracy of the results and the depth and the rate of the convergence.

Coakley [12] implemented several zero- and 2 equation models in a code for the compressible Navier-Stokes equations. The present calculations for the flow around a NACA0012 at a Reynolds number of 1.000.000 and an incidence of 0^o are compared to the other zero -equation model, the Cebeci-Smith model in ref. [12]. Figure 6.8 shows the pressure (C_p) distribution on the surface of the airfoil and fig. 6.9 shows the friction coefficient C_f. As can be seen, there exists a good agreement between solutions obtained by Coakley and the present results. Compressibility effects plays a minor role at this Reynolds number.

As discussed in a previous chapter the Baldwin-Lomax and other zero-equation turbulence models are highly grid dependent.

Three different grids were constructed to be applied for computations for the flow around a NACA0012 at a Reynolds number of 1.000.000 and an incidence of 0^o. The symmetrical grid (A) is constructed to have a y_2^+ at the trailing edge $\sim$ 10. The asymmetrical[1] grid (B) is constructed to have y_2^+ at the trailing edge $\sim$ 2, and grid (C) is constructed to have $y_2^+ \sim$ 5.

It is noticed that there is no differences between grid (B) and (C) except of the difference in the scaling of the ζ - lines coarsing the differences in y_2^+.

All grids have sufficient grid points in the boundary layer and the sub-layer is represented by 1 or 2 points.

As can be seen in figur 6.10 the convergence rate and depth is severly affected by changing between ,generally speaking, three almost identical grids.

[1]The same number of grid points has been applied for the symmetrical and the asymmetrical grid in both directions. The asymmetrical grid is constructed to have an η - line parallel to the stagnation line for the flow incidence of 8^o

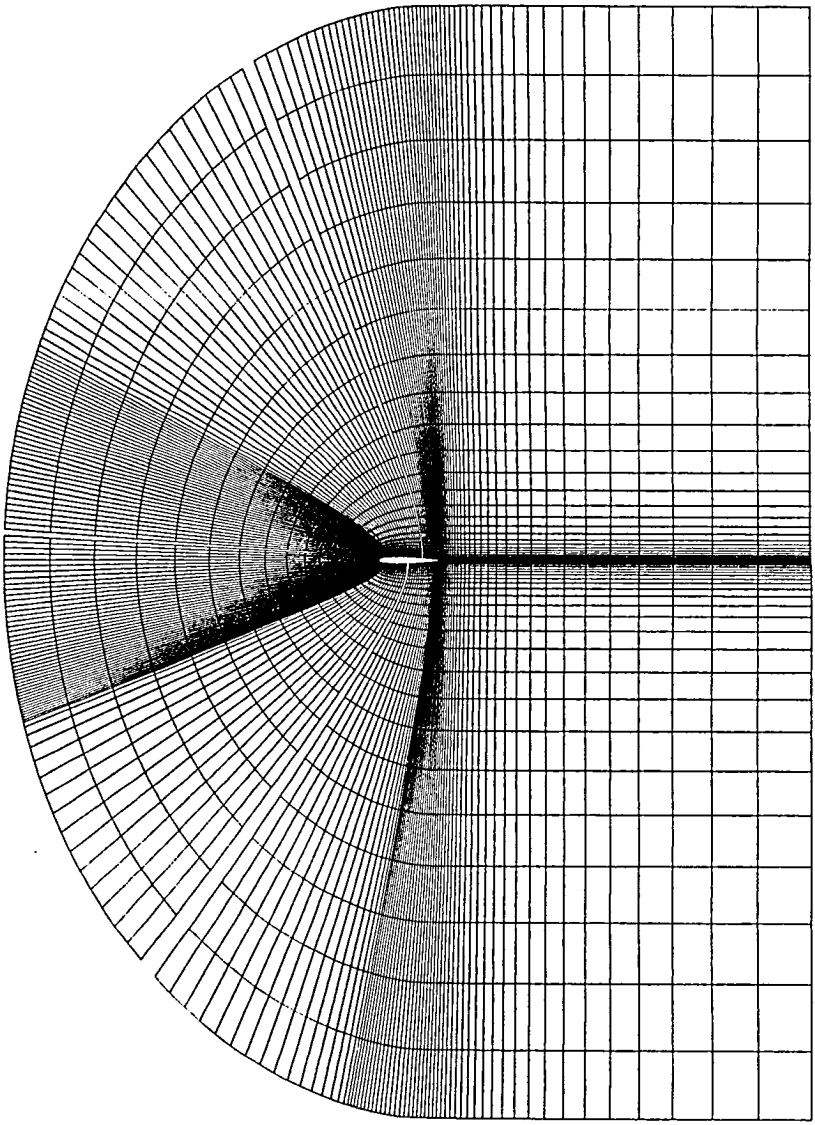

Figure 6.7: Grid around a NACA0012 airfoil applied for computations for $\mathrm{Re} = 10^6$

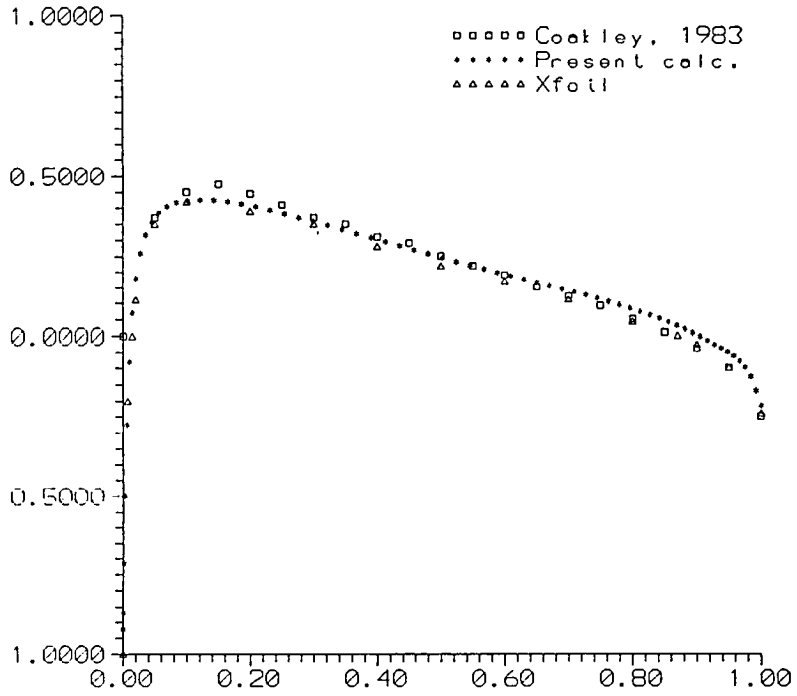

Figure 6.8: Pressure coefficient on the surface of a NACA0012 airfoil for $\mathrm{Re} = 10^6$ and $\alpha = 0°$.

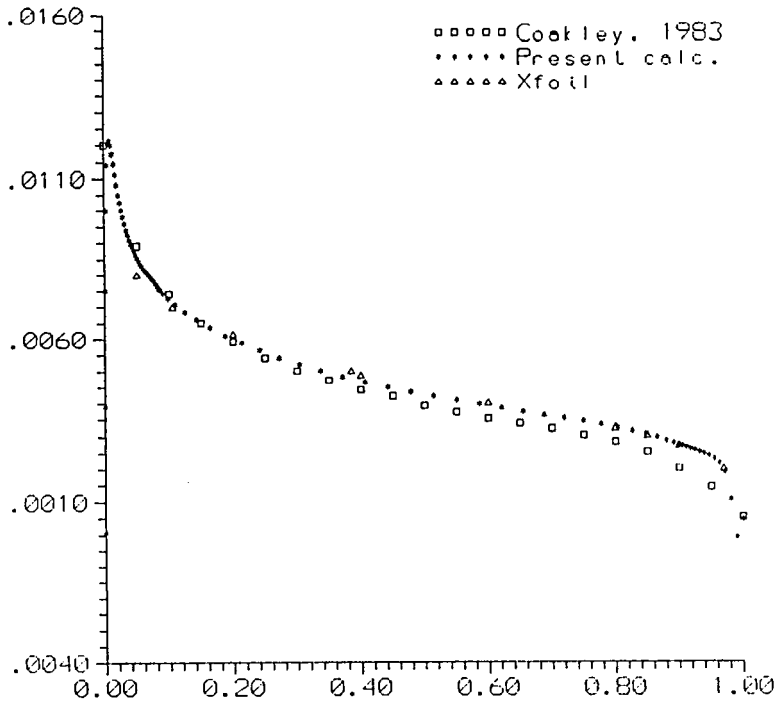

Figure 6.9: Friction coefficient on the surface of a NACA0012 airfoil for Re $= 10^6$ and $\alpha = 0°$.

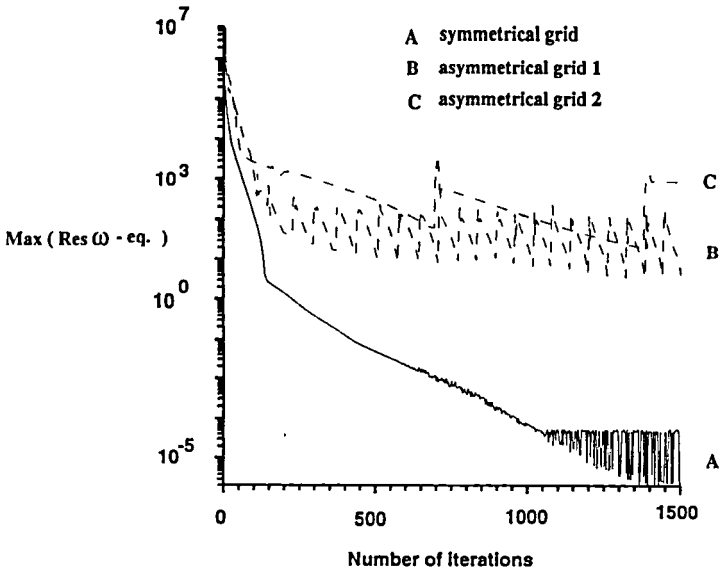

Figure 6.10: Convergence rates and depths for solutions obtained for a NACA0012 at Re $= 10^6$ and $\alpha = 0°$ applying 3 different grids.

Using the symmetrical grid (A) for this symmetrical flow gives a fast an accurate solution. For the pressure solution grid (A) and (B) produces adequate results.

The result on pressure from the computation on grid (C) differ significant from those solutions obtained on grid (A) and (B).

6.2.2 Flow around a NACA0012 airfoil at $\alpha = 8°$ and Re $= 10^6$

For the incidence of $\alpha = 8°$ and the Reynolds number of 1.000.000 a pressure solution has been compared with results from the previous mensioned integral code XFOIL. XFOIL has been used for calculations on other types of airfoils and is known to predict well compared to wind tunnel measure-

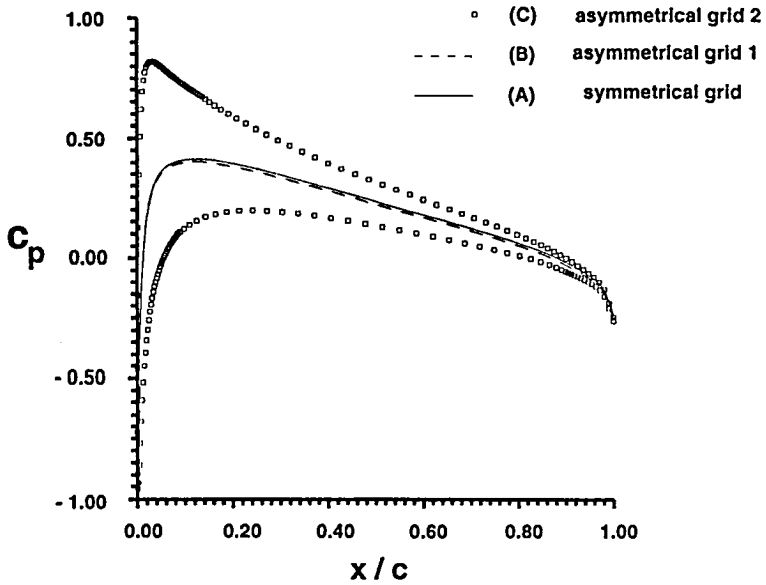

Figure 6.11: Pressure distributions for solutions obtained for a NACA0012 at Re $= 10^6$ and $\alpha = 0^o$ applying 3 different grids. The total number of iterations are the same for each solution.

ments, as will be shown later. Figure 6.12 shows a very good accordance between the present solution and the XFOIL pressure calculations.

6.2.3 Flow around a NACA0012 airfoil at $\alpha = 0^o$, 6^o, 8^o, 16^o and Re = 2.889.000

The final results on computations on the NACA0012 airfoil is at a Reynolds number of 2.889.000 and at incidences of 0^o, 6^o, 8^o and 16^o. Similar results can be found in [8], where Cebeci compares to experimental results.

6.2.4 Flow around a NTUA airfoil at $\alpha = 8^o$, $\alpha = 12^o$ and Re = 10^6

To see if the present code was able to predict pressure distributions on more irregular shaped airfoils designed with application for wind turbines, a grid as shown in fig. 6.14 was constructed.

Madsen [30] compared results from computations on the NTUA airfoil by different codes : XFOIL, FIDAP[2] and NS1[3]. Computations were done for the unseparated flow at a Reynolds number of 1.000.000 and an incidence of 8^o. The present calculations were compared to these results.

It is seen that XFOIL, applying free transition, obtains the best predictions compared to the wind tunnel measurements from the University of Southampton. Here after the present calculations, with leading edge transition, is closest. Both of the Navier - Stokes codes applying the standard κ - ε turbulence models are more off. These codes apply "The law of the wall" and the first gridline from the airfoil surface starts at $y_2^+ > 30$.

Similar results were obtained and compared for the separated flow at the NTUA airfoil at the same Reynolds number but with the incidence $\alpha = 12^o$.

Again for the 12^o XFOIL seems to predict best compared to experimental results. Present results comes second on the first 20 percent of the chord. The NS1 code and the present code do not obtain separated results. It is noticed that both of the leading edge pressure peaks in the experimental results are captured most accurate by the present solution.

[2]FIDAP is a commercial Navier - Stoke code in use at The Test Station for Wind turbines, Risø National Laboratory

[3]A Navier - Stokes code in primitive variables with a standard κ - ε turbulence model, developed by Niels N. Sørensen, The Department for Meteorology and Wind Energy, Risø National Laboratory

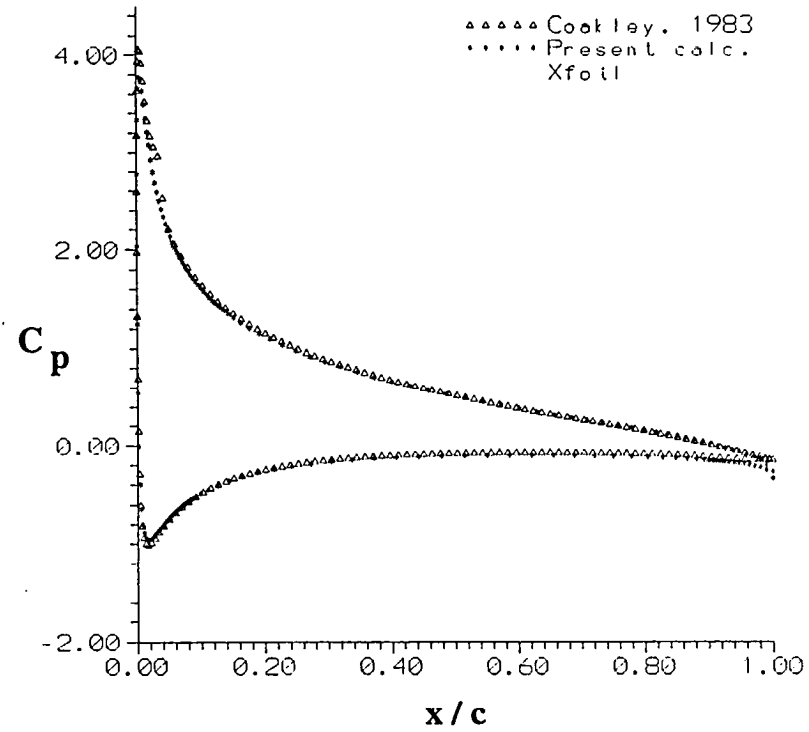

Figure 6.12: Pressure coefficient on surface of a NACA0012 airfoil for Re $= 10^6$ and $\alpha = 8°$.

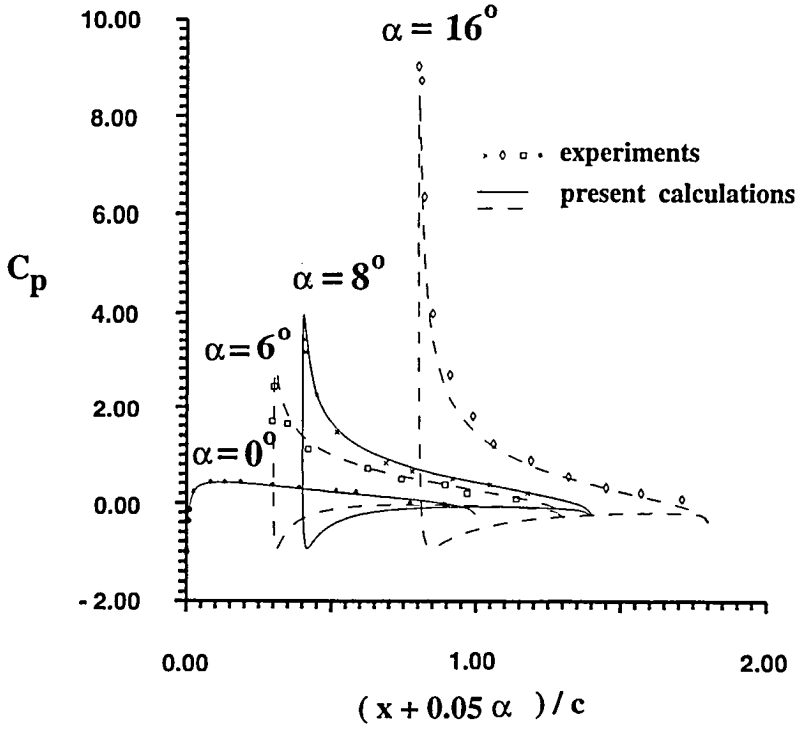

Figure 6.13: Pressure coefficient on the surface of a NACA0012 airfoil for Re = 2.889.000 and $\alpha = 0°$, $\alpha = 6°$,$\alpha = 8°$ and $\alpha = 16°$

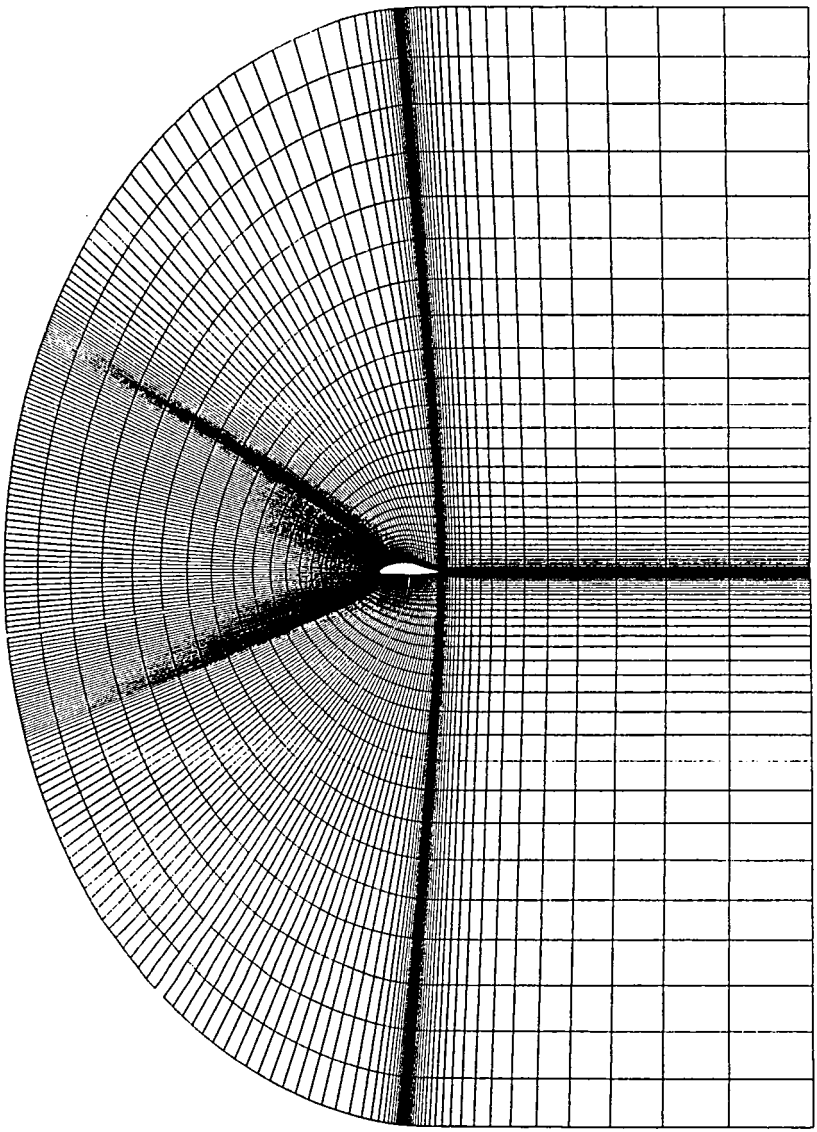

Figure 6.14: Grid around a NTUA profile applied for computations at Re $= 10^6$

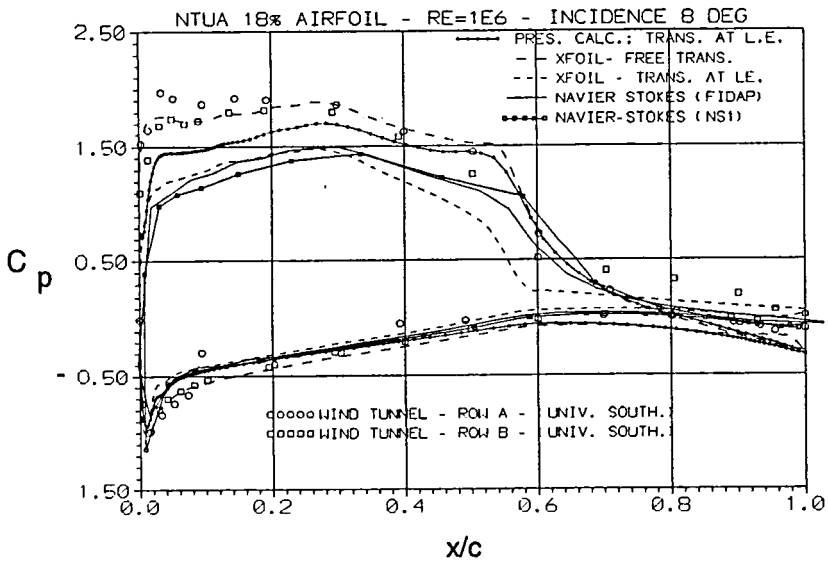

Figure 6.15: Pressure coefficient on surface of NTUA airfoil for Re = 10^6 and $\alpha = 8°$.

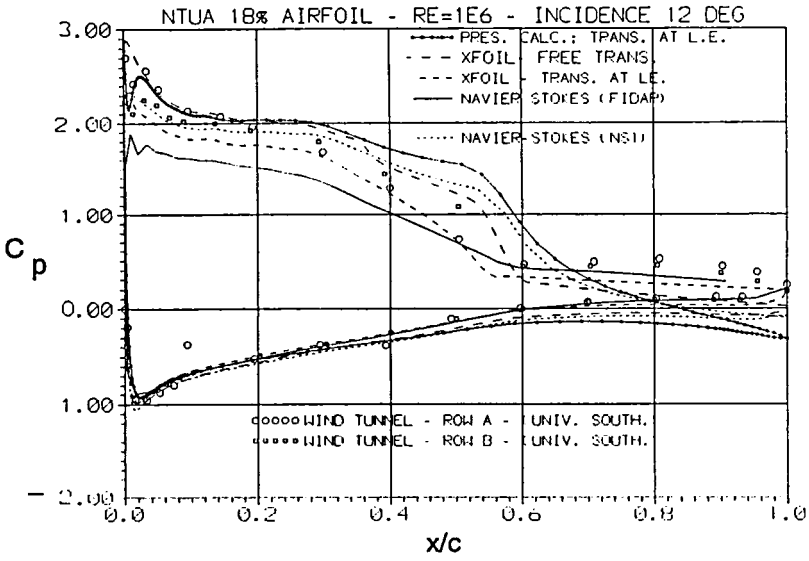

Figure 6.16: Pressure coefficient on surface of NTUA airfoil for Re = 10^6 and $\alpha = 12°$.

Chapter 7

General discussion and conclusion.

A code on a vorticity - streamfunction formulation has been developed to model the turbulent flow around airfoils designed for wind turbines.

A second order implicit boundary condition, proposed by [37] has been applied for the vorticity at the wall. A strong coupling between the vorticity transport equation and the Poisson equation for the streamfunction has been applied, resulting in a block iterative solver instead of a point iterative.

Applying a transport equation, proposed by [37] for the stagnation pressure rather than the "traditional" Poisson equation for the static pressure secure an accurate solution.

For low Reynolds numbers (laminar $\sim$ 5 - 1000) the code has been evaluated on flows around a cylinder and a NACA0012 airfoil. The results show good agreement with the literature.

For high Reynolds numbers (turbulent $\sim$ 10^6 - $3 \cdot 10^6$) the code has been tested on the NACA0012 airfoil and good agreement with literature is found.

At a Reynolds number of 10^6 predictions of the attached turbulent flow on a speciel designed airfoil to be applied for wind turbines ,the NTUA airfoil, are made. Taking into account that the present formulation do not model transition, the code predicts well compared to other uncommercial and commercial codes.

There has been an evaluation of 3 ways to compute the variables at the periodic boundary introduced by the applied C - grid. The result is that the traditional way, which is the easiest to programme, also is the numerical cheapest. The result is valuable for obtaining steady turbulent flow.

Systematic test of the connexion between generating grids and uptaining converged solutions on these grids has been made. Secondly adjustments on grids, where a converged solution is found, is done in a way to get an optimal rate of convergence, convergence depth and an accuracy of the solution.

For 3 almost similar grids around a NACA0012 airfoil (Re = 10^6 and α = 0°), it was found that the rate of convergence, the convergence depth and the accuracy of the results was significantly altered, depending on the grid applied. For this flow situation the symmetrical grid proved to be best.

Bibliography

[1] Iterative methods for sparse systems of linear equations. Version 1B 1, Numerical Institute, Techn. Univ. of Denmark, 1990.

[2] V.S. Arpaci and P.S. Larsen. *Convection Heat Transfer.* Printice Hall, Inc., Englewood Cliffs, NJ 07632, first edition, 1984.

[3] B. Baldwin and H. Lomax. Thin layer approximation and algebraic model for separated turbulent flows. *AIAA Paper 78-257*, 1978.

[4] Anders Björck. Coordinates and calculations for the ffa-w1-xxx, ffa-w2-xxx and ffa-w3-xxx series of airfoils for horisontal axis wind turbines. Technical Report TN 2990-15, Flygtekniska Försögsanstalten, 1991.

[5] C. P. Butterfield. Aerodynamic pressure and flow-visualization messurement from a rotating wind turbine blade. *Eighth ASME Wind Energy Symp., Houston, TX, pp. 245-256*, 1989.

[6] C. P. Butterfield. Three-dimensional airfoil performance measurements on a rotationg wing. *Proc. of European Wind Energy Conference Glasgow, Scotland*, 1989.

[7] T. Cebeci. Three-dimensional boundary layers. AGARD R-719, North Atlantic Treaty Organization, 1984.

[8] T. Cebeci. Computation of three-dimensional boundary layers including separation. AGARD R-741, North Atlantic Treaty Organization, 1986.

[9] T. Cebeci and A.M.O. Smith. *Analysis of Turbulent Boundary Layers.* Academic Press, 1974.

[10] P. Chaviaropoulos and K. D. Papailiou. Private communication.

[11] H. F. Christensen and H. A. Madsen. Vortex - panel metode, beregningsmodel for stroemningen omkring et profil. Risoe M-Report M-2814, Risoe National laboratory, 1989.

[12] T. J. Coakley. Turbulence modelling methods for the compressible navier-stokes equations. *AIAA*, AIAA-83-1693, 1983.

[13] S. C. R. Dennis and Gau-Zu Chang. Numerical solutions for steady flow past a circular cylinder at reynolds number up to 100. *Journal of Fluid Mechanics*, 42, 1970.

[14] M. Drela. Improvements in low reynolds number airfoil flow predictions with ises and xfoil. Technical report, Rockwell Int., Rocky Flats Plant, 1991.

[15] D. M. Eggleston and F. S. Stoddard. *Wind Turbine Engineering Design.* Van Nostrand Reinhold Company Inc., New York, 1987.

[16] R. Eppler. *Airfoil Design and Data.* Springer-Verlag, Berlin/ New York, 1990.

[17] J. D. Anderson et al. *Lecture series 1985-01 : Introduction to Computational Fluid Dynamics.* Von Karman Institute, 72 Chausse de Waterloo, 1640 Rhode Saint Genese, first edition, 1985.

[18] H. Glauert. *Aerodynamic Theory.* W. F. Durand, Vol IV Division L, Glouchester, Mass., 1976.

[19] R. E. Gormont. A mathematical model of unsteady aerodynamics and radial flow for application to helicopter rotors. Technical Report 76-67, US Army Air Mobility Res. Dev. Lab., 1973.

[20] H. Snel H. J. Van Grol and J. G. Schepers. Wind turbine benchmark exercise on mechanical loads effects on the hawt rotor aerodynamics. Volume 1 ECN-C-91-030, ECN, 1991.

[21] A. C. Hansen and C. P. Butterfield. Aerodynamics of horizontal-axis wind turbines. *Annual Review of Fluid Mechanics*, 25, 1993.

[22] H.F.Christensen. An axis symmetric general orthogonal vorticity-streamfunction for o- and c- type grids. to be published. 1993.

[23] H.F.Christensen and H.B. Jørgensen. Procedure til loesning af kombinerede sub/supersoniske stroemninger. Master's thesis, The University of Aalborg, 1988.

[24] J.C. Tannehill J.D. Anderson and R.H. Pletcher. *Comnputational Fluid Mechanics and Heat Transfer.* Hemisphere Publishing Corporation, ISBN 0-89116-471-5, first edition, 1984.

[25] Z.U.A. Warsi J.F. Thompson and C. Wayne Mastin. *Numerical Grid Generation.* Elsvier Science Publishing Co., Inc., New York, New York 10017, 1985.

[26] Y. Kallinderis and J. R. Baron. A new adaptive algorithm for turbulent flows. *Computers Fluids*, 21, 1992.

[27] Erwin Kreyszig. *Advanced Engineering Methematics.* John Wiley and Sons, Inc., fifth edition, 1983.

[28] D. Lee and R.H. Pletcher. Application of viscous-inviscid interaction methods to transonic turbulent flows. Final Report CSCL 01A G3/U2, Dept. of Fluid Mechanics, Techn. Univ. of Denmark, 1986.

[29] H. A. Madsen. Prec. of the fifth fidap users conference, chicago, usa. 1993.

[30] H. A. Madsen and H. F. Christensen. On the relative importance of rotational, unsteady and three-dimensional effects on the hawt rotor aerodynamics. *Wind Engineering*, 14, 1990.

[31] H. A. Madsen and H. F. Christensen. Unpublished results. 1990.

[32] H. A. Madsen and U. S. Paulsen. Dynamic stall on a 19 m hawt. *Prec. of Fifth IEA Symposium on Aerodynamics of Wind Turbines, Univers. of Stuttgart*, 1992.

[33] H. A. Madsen and F. Rasmussen. Private communication.

[34] J. W. McCroskey and P. F. Yaggy. Laminar boundary layers on helicopter rotors in forward flight. *AIAA Journal*, 10, 1968.

[35] P. Moin. Direct and large eddy simulations with application to flow control. *Computational Fluid Dynamics, 10-14 August, Austria*, IBM Europe Institute, 1992.

[36] N.Hirose and N. Kamiya. Blunt trailing edge analysis of supercritical airfoils by a navier-stokes code. *ICAS*, ICAS-90-6.6.3, 1990.

[37] K. Giannakoglou P. Chaviaropoulos, N. Lymberopoulos and K. D. Papailiou. A vorticity-streamfunction formulation for high reynolds, laminar, and incompressible two-dimensional flows. 1993.

[38] F. Rasmussen, S. M. Petersen, and G. Larsen. Investigations of aerodynamics, structural dynamics and fatique on danwin 180 kw. Technical report, Risoe National Laboratory, 1988.

[39] C. M. Rhie. *A numerical study of the flow past an isolated airfoil with separation.* PhD thesis, Dept. of Mech. and Ind. Eng., University of Illinois at Urbana-Champaign, 1981.

[40] J.E. Carter R.L. Davis and M. Hafez. Three-dimensional viscous flow solutions with a vorticity-stream function formulation. *AIAA Journal*, 27, 1989.

[41] P. E. Wood R.W.Yeo and A. N. Hrymak. A numerical study of laminar 90-degree bend duct flow with different discretization schemes. *Journal of Fluids Engineering*, 113, 1991.

[42] Y. Saad and M. H. Schultz. Gmres: a generalized minimal residual algorithm for solving nonsymmetric linear systems. Research Report YALEU/DCS/RR-254, Yale University, Department of Computer Science, 1983.

[43] H. Schlichting. *Boundary-Layer Theory.* McGRAW-HILL BOOK COMPANY, New York, seventh edition, 1979.

[44] J. N. Sørensen. *Three level, viscous - invicid interaction technique for the prediction of separated flow past rotating wings.* PhD thesis, The Technical University of Denmark, 1986.

[45] J. N. Sørensen. Numerical solution of the unsteady, three-dimensional and incompressible navier-stokes equations in velocity-vorticity variables. Research Report No. 16-4354.M, Dept. of Fluid Mechanics, Techn. Univ. of Denmark, 1990.

[46] J. N. Sørensen and Ta Phuoc Loc. High-order axisymetric navier-stokes code description and evaluation of boundary contitions. *International Journal for Numerical Methods in Fluids*, 9, 1989.

[47] S.V.Patankar and D.B. Spalding. A calculation procedure for heat, mass and momentum transfer in three-dimensional parabolic flows. *International Journal for Heat and Mass Transfer*, 15, 1972.

[48] C. Vuik. Solution of the discretized incompressible navier-stokes equations with the gmres method. *International Journal for Numerical Methods in Fluids*, 16, 1993.

[49] E.L. Wachpress. *Iterative Solution of Elliptic Systems.* Printice-Hall, Englewood Cliffs, N.J., first edition, 1966.

[50] Z.U.A. A note on the mathematical formulation of the problem of numerical coordinate generation. *Quarterly of Applied Mathematics*, 41, 1983.

Chapter 8

Appendices

8.1 Derivation of the $\psi - \omega$ formulation in cartesian coordinates.

The ω-ψ formulation in cartesian coordinates is derived as follows:

Definition of vorticity

$$\omega k = \nabla \times V \tag{8.1}$$

Definition of streamfunction

$$V = -\nabla \times (\psi k) \tag{8.2}$$

$$= -\begin{vmatrix} \frac{\partial}{\partial x} & \frac{\partial}{\partial y} \\ \psi & \psi \end{vmatrix}$$

$$= -\begin{vmatrix} \frac{\partial \psi}{\partial y} \\ -\frac{\partial \psi}{\partial x} \end{vmatrix}$$

Equation (8.1) and eq. (8.2) gives the relation between the vorticity ω and the streamfunction ψ :

$$\omega k = -\nabla \times \nabla \times (\psi k) \tag{8.3}$$

Before continuing the derivation of the vorticity transport equation we wish to make an assumption about ψ in order to reduce eq. (8.3).

For an incompressible flow the divergence of the velocity field and the divergence of the vorticity field equals 0 :

$$\nabla \cdot V = 0 \tag{8.4}$$

$$\nabla \cdot (\omega k) = 0 \tag{8.5}$$

Every vector field can be described by the sum of the rotation of the streamvector (3D) and the divergence of a potential function :

$$V = -\nabla \times (\psi k) + \nabla \phi \tag{8.6}$$

In this case $\nabla\ \phi = 0$ per definition.

According to the vector rule eq. (8.6) ψk again can be written as a term related to rotation and a term related to the divergence of a scalar field.

$$\psi k = -\nabla \times A + \nabla B \tag{8.7}$$

If we chose a vector function $\psi^* k$ so that $\psi^* k = \psi k$ - ∇ B , we get :

$$\psi^* k = -\nabla \times A \tag{8.8}$$

According to vector rule[1*] we obtain :

$$\nabla \cdot (\psi k) = 0 \tag{8.9}$$

By applying vector rule[2*] and keeping in mind eq.(8.9), Equation (8.3) then reduces to a Poisson equation for the streamfunction :

$$\omega = -\nabla^2 \psi \tag{8.10}$$

$$= -\left| \frac{\partial^2 \psi}{\partial x^2} + \frac{\partial^2 \psi}{\partial y^2} \right|$$

Deriviation of the vorticity transport equation

The vorticity transport equation is deriviated from the velocity transport equation

---

[1*] $\nabla.(\nabla \times A) = 0$

[2*] $\nabla \times (\nabla \times A) = \nabla \cdot (\nabla \cdot A) - \nabla^2 A$

$$\underbrace{(V \cdot \nabla)V}_{term2} = \underbrace{-\frac{1}{\varrho}\nabla p}_{term3} + \underbrace{\nu \nabla^2 V}_{term4} \tag{8.11}$$

by taking the curl of this equation. Applying the curl operator to each of the terms in eq. (8.11) we obtain :

term2:

$$\nabla \times [(V \cdot \nabla)V]^{3*} \tag{8.12}$$

$$= \nabla[(V \cdot \nabla)V] \times V + (V\nabla)(\nabla \times V)$$

$$= \nabla V \cdot (\nabla \times V) + (V\nabla)(\omega k)$$

$$= -[(\omega k)\nabla]V + [V\nabla](\omega k)$$

term3:

$$\nabla \times [-\frac{1}{\rho}\nabla p] = 0^{4*} \tag{8.13}$$

term4:

$$\nabla \times [\nu \nabla^2 V] = \nu \nabla^2 (\nabla \times V) = \nu \nabla^2 (\omega k) \tag{8.14}$$

Which gives the vorticity transport equation

$$[V\nabla](\omega k) = [(\omega k)\nabla]V + \nu \nabla^2 (\omega k) \tag{8.15}$$

$^{3*} \nabla \times (U \cdot A) = \nabla \cdot (\nabla U) \times A + U(\nabla \times A)$

$^{4*} \nabla \times (\nabla U) = 0$

8.1.1 Introduction of dimensionless variables.

The system of equation is made dimensionless by introducing the dimensionless variables related to a characteristic length L_0 and velocity V_0 :

$$\left| \begin{array}{ll} x^* = \frac{x}{L_0} & y^* = \frac{y}{L_0} \\ u^* = \frac{u}{V_0} & v^* = \frac{v}{V_0} \\ \psi^* = \frac{\psi}{V_0 L_0} & \omega^* = \frac{\omega L_0}{V_0} \\ Re_l = \frac{L_0 V_0}{\nu} & \end{array} \right| \tag{8.16}$$

8.2 Transformation of the governing equations from a cartesian coordinate system to a general curvelinear coordinate system

To present the governing equations on a form which is satisfactory with respect to the numerical solution of the equations, they have to be transformed from a cartesian coordinate system (physical domain) to a general curvelinear coordinate system (computational domain).

The relations needed for this transformation is based on concepts from differential geometry and tensor analysis, and an extensive collection of concepts from the two fields can be found in [50]. Here we only present the definitions of relations needed to understand the basic transformation, on the form given in [25].

Vector bases

Transformation

$$(x^1, x^2, x^3) \mapsto (u^1, u^2, u^3) \tag{8.17}$$

$$x^1 = x, x^2 = y, x^3 = z \tag{8.18}$$

$$u^1 = \zeta, u^2 = \eta, u^3 = \xi \tag{8.19}$$

$$r = xi + yj + zk \tag{8.20}$$

Covariant

$$g_i = \frac{\partial r}{\partial u^i}, i = 1, 2, 3 \tag{8.21}$$

$$g_i = (\frac{\partial x}{\partial u^i}, \frac{\partial y}{\partial u^i})^T \tag{8.22}$$

Contravariant

$$g^i = \nabla u^i \tag{8.23}$$

$$g^i = (\frac{\partial u^i}{\partial x}, \frac{\partial u^i}{\partial y})^T \tag{8.24}$$

Relations between co-and contra variant vector bases

$$g_1 \perp g^2 \tag{8.25}$$

$$g_2 \perp g^1 \tag{8.26}$$

$$g^i g_i = \delta^i_j \tag{8.27}$$

Covariant metric tensor

$$g_{ij} = g_i g_j \tag{8.28}$$

Contravariant metric tensor

$$g^{ij} = g^i g^j \tag{8.29}$$

Relations between co- and contra variant metric tensor

$$g_{ij} g^{jk} = \delta_j^k \tag{8.30}$$

Jacobian 2D

$$J = \mid g_1 x g_2 \mid = x_\zeta y_\eta - x_\eta y_\zeta \tag{8.31}$$

Distances 2D

$$\mid ds \mid^2 = \frac{\partial r}{\partial u^i} du^i \frac{\partial r}{\partial u^j} du^j = g_i g_j du^i du^j, i = 1, 2 \tag{8.32}$$

Cartesian velocities

$$\boldsymbol{V} = g_i v^i \tag{8.33}$$

$$\boldsymbol{V} = g^i v_i \tag{8.34}$$

$$\mid \boldsymbol{V} \mid^2 = \boldsymbol{V}\boldsymbol{V} = g^i v_i g_j v^j = v_i v^j \delta_j^i = v_i v^j \tag{8.35}$$

Transformation of operators related to the governing equations

The governing equations (8.36) and (8.37) , represented in a cartesian coordinate system need to be transformed to a general curvelinear coordinate system to be on a form satisfactory to the numerical solution. The divergence and laplacian operators is applied on a conservation form, to remove stability restrictions related to the inversion of the factorised matrices

$$\nabla^2\psi + \omega = 0 \tag{8.36}$$

$$\nabla(V\omega k) - \frac{1}{Re_l}\nabla^2[(1 + \frac{Re_l}{Re_t})\omega k] = 0 \tag{8.37}$$

In the following the different operators in the governing equations is transformed

gradient

$$\nabla() = g^i\frac{\partial()}{\partial u^i} \tag{8.38}$$

transport term

$$\nabla[V()] = v^i g_i g^j \frac{\partial()}{\partial u^j} = v^i \delta_i^j \frac{\partial()}{\partial u^i} \tag{8.39}$$

Divergence on conservation form

$$\nabla\cdot V = \frac{1}{J}\frac{\partial(Jv^i)}{\partial u^i} \tag{8.40}$$

Laplacian on conservation form

$$\nabla \cdot \nabla \psi = \frac{1}{J} \frac{\partial}{\partial u^i} (J g^{ij} \frac{\partial \psi}{\partial u^j}) \tag{8.41}$$

8.3 Derivation of the transport equation for static pressure.

The transport equation for the static pressure is derived from the velocity trans port equation :

$$\underbrace{(V \cdot \nabla) V}_{term1} = \underbrace{-\frac{1}{\rho} \nabla p}_{term2} + \underbrace{\nu \nabla^2 V}_{term3} \tag{8.42}$$

The *term2* is rewritten and the total pressure p is replaced by the static pressure p_t.

term2 :

$$-\frac{1}{\rho} \nabla p^{5*} = -\frac{1}{\rho} \nabla p_t + \frac{1}{2} \nabla [V \cdot V]^{6*} = \tag{8.43}$$

$$\frac{1}{\rho} \nabla p_t + V \cdot \nabla V + V \times \omega k \tag{8.44}$$

term3 :

$$\nu (\nabla^2 V)^{7*} = \nabla \cdot (\nabla \cdot V)^{8*} - \nabla \times (\nabla \times V) = \tag{8.45}$$

$$-\nu (\nabla \times \omega \cdot k) \tag{8.46}$$

Equation (8.42) then takes the form :

$$\rho (V \times \omega k) = \nabla p_t - \mu (\nabla \times \omega k) \tag{8.47}$$

$^{5*} p = p_t - \frac{1}{2} \rho V^2$

$^{6*} \nabla (A \cdot B) = (B \cdot \nabla) A + (A \cdot \nabla) B + B \times (\nabla \times A) + A (\nabla \times B)$

$^{7*} \nabla \times (\nabla \times A) = \nabla \cdot (\nabla \cdot A) - \nabla^2 A$

$^{8*} \nabla \cdot V = 0$

Which on dimensionless form (applying the previous mensioned dimensionless parameters given in Appendix 8.2) is :

$$\rho(V \times \omega k) = \nabla p_t - \frac{1}{Re}(\nabla \times \omega k) \tag{8.48}$$

Equation (8.48) is multiplied by V :

$$V \cdot \rho(V \times \omega k)^{9*} = V \nabla p_t - \frac{1}{Re}(V \nabla \times \omega k) \tag{8.49}$$

leading to the equation :

$$V \nabla p_t - \frac{1}{Re}(V \nabla \times \omega k) = 0 \tag{8.50}$$

In order to obtain a transport equation for p_t the divergence is taken of eq. (8.48) :

$$\nabla[\rho(V \times \omega k)]^{10*} = \nabla[\nabla p_t - \frac{1}{Re}(\nabla \times \omega k)] \tag{8.51}$$

which gives :

$$\rho \omega k \cdot \omega k - \rho \cdot V(\nabla \times \omega k) = \nabla^2 p_t - \frac{1}{Re}\nabla(\nabla \times \omega k)^{11*} \tag{8.52}$$

giving

$$\rho \omega^2 - \rho V(V \times \omega k) = \nabla^2 p_t \tag{8.53}$$

Combining eq. (8.50) and (8.53) gives :

$$\rho V \cdot \nabla p_t - \frac{1}{Re}\nabla^2 p_t = -\frac{1}{Re}\rho \omega^2 \tag{8.54}$$

$^{9*} V \cdot (V \times \omega k) = 0$
$^{10*} \nabla(A \times B) = B(\nabla \times A) - A \cdot (\nabla \times B)$
$^{11*} \nabla(\nabla \times A) = 0$

8.4 ADI - Incomplete factorization

In order to uptain an iterative solution to the system of the unlinear governing equations and related boundary conditions the Newton linearized governing equation is put on a form ideal to the solution by an ADI (Alternating Direction Implicit) scheme.

The system of each of the governing equations in the computational domain can be put on the following principal form, which constitutes the basic form of the equations solved by an ADI scheme :

$$(\frac{\underline{I}}{\Delta t} + \underline{A} + \underline{B})x = b \tag{8.55}$$

where Δt is a pseudo time step related to the solution by iteration in the pseudo time domain. Δt is different for the Poisson equation and the transport equation, respectively Δt_ψ and Δt_ω. $\underline{I}$ is a unity matrix and $\underline{A}$ and $\underline{B}$ is matrices consisting of matrix elements containing differential operators that works respectively with respect to the ζ-direction and the η-direction. x is the solution vector containing the unknown variables ($\Delta\psi$ or $\Delta\omega$) for the flow domain.

Equation (8.55) represents respectively the elements A_{11} and A_{22} in the Jacobian matrix arriving from the Newton linearisation of the governing equations.

Written out A_{11} becomes :

$$A_{11} = \frac{\underline{I}}{\Delta t_\psi} + \frac{1}{J}\frac{\partial}{\partial\zeta}[Jg^{11}\frac{\partial}{\partial\zeta}() + Jg^{12}\frac{\partial}{\partial\eta}()] + \frac{\partial}{\partial\eta}[Jg^{21}\frac{\partial}{\partial\zeta}() + Jg^{22}\frac{\partial}{\partial\eta}()] \tag{8.56}$$

Due to an optimal representation of A_{11} with respect to the Newton scheme the mixed derivatives are left out. A_{11} then becomes :

$$A_{11} = \frac{\underline{I}}{\Delta t_\psi} + \frac{1}{J}\frac{\partial}{\partial\zeta}[Jg^{11}\frac{\partial}{\partial\zeta}()] + \frac{\partial}{\partial\eta}[Jg^{22}\frac{\partial}{\partial\eta}()] \tag{8.57}$$

Similar A_{22} is written out and becomes :

$$A_{22} = \frac{\underline{I}}{\Delta t_\omega} + \frac{\partial}{\partial\zeta}[v^1()] - \frac{1}{ReJ}\frac{\partial}{\partial\zeta}[Jg^{11}\frac{\partial}{\partial\zeta}()] + \frac{\partial}{\partial\eta}[v^2()] - \frac{1}{ReJ}\frac{\partial}{\partial\eta}[Jg^{22}\frac{\partial}{\partial\eta}()] \tag{8.58}$$

The form of eq. (8.55) or eq. (8.57) or eq. (8.58) will for a 2nd order discretized scheme represent a pentadiagonal matrix. This matrix is normally factorized into 2 tridiagonal matrices.

The ADI scheme applied make use of an approximated factorization of eq. (8.55). This approximation leaves out 2nd order terms with respect to time :

$$(\underline{I} + \Delta t\underline{A} + \Delta t\underline{B}) = (\underline{I} + \Delta t\underline{A})(\underline{I} + \Delta t\underline{B}) + \Delta t^2 \underline{AB} \simeq \tag{8.59}$$

$$(\underline{I} + \Delta t\underline{A})(\underline{I} + \Delta t\underline{B}) \tag{8.60}$$

The similar approximated factorized representation of A_{11} and A_{22} gives the inverted elements of the preconditioning matrix $\underline{P}$:

$$\underline{P^n} = \begin{bmatrix} P_{11}^{-1} & -P_{11}^{-1}P_{22}^{-1} \\ 0 & P_{22}^{-1} \end{bmatrix} \tag{8.61}$$

and

$$P_{11} = -\frac{1}{\Delta t_\psi}\{I - \frac{\Delta t_\psi}{J}(Jg^{11}\frac{\partial}{\partial\zeta}())\}\{I - \frac{\Delta t_\psi}{J}(Jg^{22}\frac{\partial}{\partial\eta}())\} \tag{8.62}$$

and

$$P_{22} = -\frac{1}{\Delta t_\omega}\{I + \Delta t_\omega(\frac{\partial}{\partial\zeta}[()v^1] - \frac{1}{JRe_l}\frac{\partial}{\partial\zeta}(Jg^{11}\frac{\partial}{\partial\zeta}([1 + \frac{Re_l}{Re_T}]()))\}$$

$$\{I + \Delta t_\omega(\frac{\partial}{\partial\eta}[()v^2] - \frac{1}{JRe_l}\frac{\partial}{\partial\eta}(Jg^{22}\frac{\partial}{\partial\eta}([1 + \frac{Re_l}{Re_T}]()))\} \tag{8.63}$$

8.5 Components of the GMRES method

8.5.1 Subspace methods

The basic concepts of a subspace method is described here in order to understand the nature of the GMRES-method.

The system of equation :

$$\underline{A}x^* = b, \qquad k = 0, 1, 2... \tag{8.64}$$

giving the initial vector x_0 have the residual vector :

$$r_0 = b - \underline{A}x_0 \tag{8.65}$$

can be expressed as :

$$\underline{A}x^* - x_0 = r_0, \tag{8.66}$$

This formulation of the problem is the most convenient one for the purpose of introducing subspace methods.

Let V_k and W_k be k-dimensional subspaces of R^n . Let v_1, v_2,....,v_k and w_1, w_2, ...,w_k be basis vectors of V_k and W_k, that is respectively they are linearly independent.

Let

$\underline{V} = [v_1, v_2, ..., v_k]$

and

$\underline{W} = [w_1, w_2, ..., w_k]$

($\underline{V}$ and $\underline{W}$ are (n x k) matrices. We seek an approximation to x^* of the form :

$$x_k = x_0 + c_1 v_1 + c_2 v_2 + ...c_k v_k = x_0 + \underline{V}c \tag{8.67}$$

Already at this point a similarity can be seen between x_k and $\underline{V}c$ as a relation between a vector and its eigenvector. Later on it will be shown that c, $\underline{V}$ and $\underline{W}$ will not be arbitrary chosen.

Unless by chance $x^* - x_0 \in V_k$, there is no vector x_k that satisfies eq. 8.66 .

On the other hand, we can usually determine a vector x_k of form like (8.67) by requiring that :

$$w_i^T \underline{A}(x_k - x_0) = w_i^T r_0 \qquad i = 1, 2, ...k \tag{8.68}$$

or more compact

$$(\underline{W}^T \underline{AV})c = W^T r_0 \qquad i = 1, 2, ...k \tag{8.69}$$

The *subspace method* based on V_k and W_k is thus defined as follows :

$$(W^T \underline{AV})c^* = W^T r_0 \qquad (solve\ for\ c^*) \tag{8.70}$$

$$x_k = x_0 + \underline{V}c^* \tag{8.71}$$

Where it can be shown that $w^T r_k = 0$ for all $w \in W_k$.

8.5.2 Iterative formulation of subspace methods

An iterative formulation of subspace methods, where the assumption

$$w_i^T \underline{A} v_j = 0, \qquad i \neq j \tag{8.72}$$

$$w_i^T \underline{A} v_j \neq 0, \qquad i = j \tag{8.73}$$

gives c_i :

$$c_i = \frac{w_i^T r_0}{(w_i^T \underline{A} v_i)}, \qquad i = 1, 2, .., k \tag{8.74}$$

can be formed as :

$$a_i = \frac{-w_i^{*T}(\underline{A} v_k)}{(w_i^{*T} \underline{A} v_i^*)}, \qquad i = 1, 2, .., k-1 \tag{8.75}$$

$$v_k^* = a_1 v_1^* + a_2 v_2^* + ...a_{k-1} v_{k-1}^* + v_k + \underline{V} c \tag{8.76}$$

$$z_k = a_1 z_1 + a_2 z_2 + ...a_{k-1} z_{k-1}^+ (\underline{A} v_k) \tag{8.77}$$

$$b_i = \frac{-w_k^T z_i}{w_i^{*T} \underline{A} v_i^*}, \qquad i = 1, 2, .., k-1 \tag{8.78}$$

$$w_k^* = b_1 w_1^* + b_2 w_2^* + ...b_{k-1} w_{k-1}^* + w_k \tag{8.79}$$

$$c_k = w_k^{*T} r_0 / (w_k^{*T} z_k), \qquad i = 1, 2, .., k \tag{8.80}$$

$$x_k = x_{k-1} + c_k v_k^* \qquad k = 1, 2, 3, ... \tag{8.81}$$

8.5.3 Krylov subspaces

Of special interest to the GMRES-method is the Krylov subspace, where $V_k = K_k$ and :

$$K_k = SPAN^{12}[r_0, \underline{A} r_0, ..., \underline{A}^2 r_0, ..., \underline{A}^{k-1} r_0], \qquad k = 1, 2, 3, ... \tag{8.82}$$

[12] All set of linear combinations is called the SPAN of

8.5.4 Eigen value problems

Given a linear relation :

$$\underline{A}x = b \tag{8.83}$$

Does there exist a real vector $x \neq 0$ for which the corresponding vector b is real and has the same direction and sence as x ? This is the same as saying that we want to find a vector x such that :

$$\underline{A}x = \lambda x = b \tag{8.84}$$

Clearly such a vector exists if and only if $\underline{A}$ has a real an positive eigenvalue. x is then an eigenvector corresponding to that eigenvalue.

Equation (8.84) put on another form gives :

$$[\underline{A} - \lambda \underline{I}]x = 0 \tag{8.85}$$

Stated by Cramer's theorem in [27] this homogeneous system of linear equations has a nontrivial solution if and only if the corresponding determinant of the coefficients is zero :

$$D(\lambda) = det[\underline{A} - \lambda \underline{I}] = 0 \tag{8.86}$$

By developing $D(\lambda)$ we obtain a polynomial of n'th degree in λ

8.5.5 Preconditioning

When a subspace method is used to solve a linear system

$$\underline{A}x = b \tag{8.87}$$

with $V_k = K_k$ (the Krylov subspace) then as given in [1] the optimal accuracy depends on how the eigenvalues of $\underline{A}$ are distributed in the complex plane. In particular, when the eigenvalues are real and positive.

$$0 < \lambda_1 \leq \lambda_2 \leq ..... \leq \lambda_n \tag{8.88}$$

then [1] establish that the parameter

$$\kappa = \frac{\lambda_n}{\lambda_1} \geq 1 \tag{8.89}$$

is important. The smaller the value of κ, the better the solution x can be approximated in the set $x_0 + K_k$. Clustering of eigenvalues tends to increase accuracy (also when the eigenvalues are not real and positive).

If a splitting of $\underline{A}$ is given :

$$\underline{A} = \underline{M} - \underline{N} \tag{8.90}$$

a preconditioning of 8.87 could be :

$$\underline{M}^{-1}\underline{A}\boldsymbol{x} = \underline{M}^{-1}\boldsymbol{b} \tag{8.91}$$

A legitimate question to ask is how should the preconditioning matrix be found in order to get it optimal with respect to solving the original equation (8.84) ?

Two criterias can be mensioned :

1) The spectral radius[13] $\rho(\underline{G})$, $(\underline{G} = \underline{M}^{-1}\underline{N})$ should be small.

2) It is efficient to solve a system of equations having $\underline{M}$ as a coefficient matrix. since these are the same properties that characterize a good splitting, (e.g. $\underline{A} = \underline{M} - \underline{N}$ or $\underline{A}$ is factorized in some way) for a stationary iterative method, such methods provide candidates for the preconditioning matrix $\underline{M}$.

8.5.6 Convergence and error definition

Error definition

When an iterative method is applied to a nonsingular linear system og equations like :

$$\underline{A}\boldsymbol{x} = \boldsymbol{b} \tag{8.92}$$

It produces a vector sequence $\boldsymbol{x}_0$, $\boldsymbol{x}_1$, $\boldsymbol{x}_2$ ... that (hopefully) converges to $\boldsymbol{x}$. To get an estimation of how close we are to a converged solution different error definitions can be applied :

$$\boldsymbol{e}_k = \boldsymbol{x}_k - \boldsymbol{x}, \qquad k = 0, 1, 2... \tag{8.93}$$

$\boldsymbol{e}_k$ is usually the error we want to know, but since the solution $\boldsymbol{x}$ in general applications is unknown, this error cannot be found. It is of interest though when comparing different iterative methods, where a seeked solution can be known.

A corresponding *average reduction factor per iteration* γ_k is defined together with the *average rate of convergence* R_k :

$$\gamma_k = [\| \boldsymbol{e}_k \| / \| \boldsymbol{e}_0 \|]^{\frac{1}{k}} \tag{8.94}$$

[13]The *spectral radius* of any square finite matrix $\underline{A}$ is defined as the magnitude of the eigenvalue of $\underline{A}$ of largest magnitude $\rho(\underline{A}) = max \mid \lambda_i(\underline{A}) \mid$

More general applied error factors are :

$$r_k = b - \underline{A}x_k, \qquad k = 0, 1, 2... \tag{8.95}$$

$$d_k = x_k - x_{k-1}, \qquad k = 1, 2, 3... \tag{8.96}$$

, where r_k is naturally applied here for the Newton iterative GMRES-solver.

Convergence

To monitor the progress of convergence of an iterative solution method, to compare different ones and to estimate when to stop the iteration one defines respectively an *average rate of convergence* R_k and a stop criteria δ or ϵ :

$$R_k = -ln(\gamma_k) \tag{8.97}$$

For ideal tests where x is known the stop criteria is :

$$\| e_k \| < \delta_1 \tag{8.98}$$

but for general applications :

$$\| r_k \| < \epsilon_1 \tag{8.99}$$

and

$$\| d_k \| < \epsilon_2 \tag{8.100}$$

8.5.7 The GMRES-algorithm

The algorithm has the following form :

1. Start : Choose x_0 and compute $r_0 = f - Ax_0$ and $v_1 = r_0 / \| r_0 \|$.

2. Iterate : For j = 1, 2, ...k,.. until satisfied do :

$h_{i,j} = (Av_j, v_j), i = 1, 2, ..., j,$

$\hat{v}_{j+1} = Av_j - \sum_{i=1}^{j} h_{i,j} v_i$, where $h_{j+1,j} = \| \hat{v}_{j+1} \|$, and $v_{j+1} = \hat{v}_{j+1} / h_{j+1,j}$

3. Form the approximate solution :

$x_k = x_0 + V_k y_k, where y_k$ minimizes :

$J(y) = \| \beta e_1 - \bar{H}_k y \|$, where

e_i is the first column of the (k+1)x(k+1) identity matrix and $\bar{H}_k$ is a matrix whose only nonzero elements are those elements $h_{i,j}$ generated by the method.